Edelweiss Applied Science and Technology
ISSN: 2576-8484
Vol. 10, No. 9, 21-53
2026
Publisher: Learning Gate
DOI: 10.55214/2576-8484.v10i9.13548

Advances in hyperthermia applicators for skin and superficial cancer treatment: A comprehensive review report

Amiruddin Shams[1*], Amanpreet Kaur[2], Arnab Pattanayak[3]
[1,2,3]Department of Electronics & Communication Engineering (ECED), Thapar Institute of Engineering & Technology, Patiala, Punjab – 147004 India; amiruddin.shams@thapar.edu (A.S.) amanpreet.kaur@thapar.edu (A.K.) arnab.pattanayak@thapar.edu (A.P.).

Abstract: Skin and superficial cancers remain major global health concerns, demanding effective, minimally invasive, and non-invasive therapies with improved precision and patient safety. Conventional treatment approaches, including surgery, chemotherapy, radiotherapy, and immunotherapy, often cause significant side effects and exhibit limited therapeutic selectivity. Microwave hyperthermia has emerged as a promising complementary treatment that selectively elevates tumor temperatures to 40–45°C without ionizing radiation. This review article aims to comprehensively summarize the evolution of microwave hyperthermia applicators reported between 1990 and 2026 for skin and superficial cancer treatment. The paper presents a comprehensive review and comparative analysis of published work covering cancer fundamentals, microwave–tissue interactions, microwave frequency bands, critical design constraints, and reported invasive and non-invasive applicators. Their electromagnetic characteristics, thermal performance, penetration capability, effective field size, and experimental validations are comparatively evaluated. The review reveals that recent developments increasingly emphasize compact, flexible, dual-band, patient-conforming, and metamaterial-based applicators that improve treatment efficiency, heating localization, and clinical practicality. It is concluded that continued advancements in applicator design are essential for improving microwave hyperthermia performance. The findings provide practical design guidance for researchers, engineers, and clinicians developing next-generation microwave hyperthermia applicators for effective skin and superficial cancer therapy.

Keywords: *Cancer treatment, Electromagnetic heating, Hyperthermia applicators, Microwave hyperthermia, Skin cancer, Thermal treatment of cancer.*

1. Introduction

Cancer is one of the leading diseases worldwide [1] and causes death. It is characterized by the uncontrolled growth of abnormal cells that affect surrounding tissues and spread to distant organs. There are various types of cancer, such as skin, breast, lung, stomach, liver, kidney, etc. Most deaths are caused by lung cancer, as reported in [2]. Skin cancer is one of the most common types of cancer. It primarily develops due to prolonged exposure to ultraviolet (UV) radiation and other environmental factors. The major types of skin cancer, including basal cell carcinoma (BCC) and squamous cell carcinoma (SCC), are classified as non-melanoma and melanoma skin cancers [3]. Skin cancer originates in the epidermis and can spread to surrounding tissues if not detected and treated early. Various non-invasive diagnostic methods, such as CT scans, chest X-rays, ultrasounds, etc., are available to examine skin cancer. However, they are limited by early-stage detection and by the use of ionizing radiation, which may pose health risks with repeated exposure. Apart from these, invasive diagnostic procedures such as positron emission tomography (PET) scans and shave biopsies may cause infections due to the

History: Received: 2 June 2026; Revised: 4 August 2026; Accepted: 7 August 2026; Published: 4 September 2026
* Correspondence: amanpreet.kaur@thapar.edu

injection of radioactive glucose into a vein and the use of a sterile razor blade to shave off abnormal cells. Various treatment methods are currently available for skin cancer, including surgery, radiation therapy, chemotherapy, immunotherapy, and photodynamic therapy [4]. Surgical excision is the most commonly used technique and is highly effective for localized tumors [5]. Radiation therapy is often used when surgery is not feasible, while chemotherapy and immunotherapy are applied in advanced or metastatic cases. However, these conventional treatments have several limitations. Surgical procedures may lead to cosmetic disfigurement and are not suitable for all tumor locations. Radiation and chemotherapy can cause significant side effects, such as damage to healthy tissues, fatigue, and immune suppression. Furthermore, some tumors develop resistance to these therapies, reducing their effectiveness over time. To overcome these limitations, microwave-based imaging techniques attract researchers due to their non-invasive and non-ionizing radiation characteristics, sufficient penetration depth, and high resolution. They can provide affordable tissue diagnosis at the early stage of skin cancer [6].

Meanwhile, many researchers have reported that the hyperthermia system is a promising invasive, non-invasive, and non-ionizing technique for treating skin cancer. In the late 1970s, the use of microwaves began for the thermal treatment of cancer [7]. Hyperthermia is defined as a thermal treatment in which body tissues are exposed to elevated temperatures to damage or kill cancer cells. It enhances the effectiveness of other therapies, such as radiation and chemotherapy. The tumor tissues are heated to temperatures in the range of approximately 40–45°C (up to 113 °F), which can selectively affect cancer cells due to their higher sensitivity to heat. Hyperthermia can be classified into three main categories: local, regional, and whole-body hyperthermia, depending on the extent of the treated area [8, 9]. Among these, local hyperthermia is particularly suitable for skin cancer treatment. It targets superficial tumors using external energy sources such as microwaves, radiofrequency, and ultrasound waves. This localized heating approach enables controlled energy delivery to tumor tissues while minimizing damage to surrounding healthy cells [10, 11].

Although microwave hyperthermia has shown significant potential for skin cancer treatment [12], several technical challenges limit its widespread clinical implementation. The effectiveness of hyperthermia depends on precise electromagnetic energy deposition within the tumor region while minimizing unintended heating of surrounding healthy tissues. This requires the careful design of antenna and microwave applicators with appropriate operating frequency, penetration depth, impedance matching, radiation characteristics, and specific absorption rate (SAR) distribution. Factors such as tissue heterogeneity, variations in dielectric properties, tumor size and depth, and patient-specific anatomical differences complicate treatment planning. In addition, maintaining uniform temperature distribution within the therapeutic range of 40–45°C remains a major challenge. Excessive heating may damage healthy tissues, whereas insufficient heating reduces therapeutic effectiveness. Therefore, the development of an efficient microwave hyperthermia system requires optimization of antenna structures, treatment monitoring techniques, and numerical modeling approaches to ensure safe and effective therapy delivery.

Figure 1 explains the effect of hyperthermia on deep-seated tumors, which are being treated using chemotherapy or ionization therapy. Also, in an early stage of cancer, heat treatment using hyperthermia therapy leads to protein damage and, hence, cell death [13]. This review paper presents a comprehensive overview of microwave-based hyperthermia systems for the treatment of skin and other superficial cancers. The paper particularly covers the reported antenna design methodologies, operating frequency selection, electromagnetic-thermal modeling techniques, and recent advancements in applicator technologies.

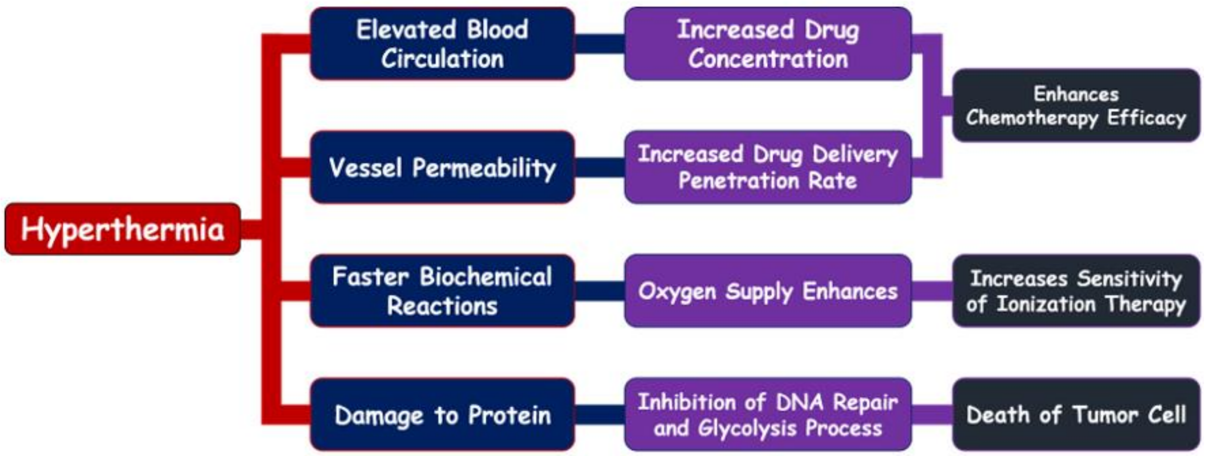

Figure 1.
Effect of Hyperthermia on Deep-Seated Tumors.

2. Experimental Microwave Hyperthermia Applicator, Constraints

Microwave hyperthermia (MHT) is an emerging cancer treatment technique that utilizes microwave-generated heat to destroy tumor cells. This method offers rapid energy delivery, controlled heating, and selective targeting characteristics. Microwave energy is delivered through a specialized antenna-based applicator at a specific frequency chosen based on tumor depth.

2.1. Microwave Frequency Bands

Table 1 summarizes the microwave frequency bands commonly employed in hyperthermia applications, along with their typical operating frequencies, penetration depths, and hyperthermia applications. In antenna-based hyperthermia (HT) systems, the selection of operating frequency is critical and typically restricted to the Industrial, Scientific, and Medical (ISM) bands, such as 434 MHz, 915 MHz, 2.45 GHz, and 5.8 GHz [13]. This is because of regulatory compliance and suitability for biomedical applications. Lower ISM frequencies, 434 MHz and 915 MHz, provide greater penetration depth, making them suitable for deep-seated tumors, whereas higher frequencies, 2.45 GHz and 5.8 GHz, offer better spatial resolution and localized heating, which is advantageous for superficial cancers, such as skin cancer [14].

Table 1.
Microwave Frequency Bands (VHF = Very High Frequency, UHF = Ultra High Frequency).

Frequency Bands	Frequency Range	Typical Operating Frequency	Penetration Depth	Hyperthermia Applications
VHF	30 – 300 MHz	70 – 150 MHz	> 10 cm	Deep Regional Hyperthermia
UHF	300 – 1000 MHz	434, 915 MHz	3 – 8 cm	Deep-Seated Tumors
L-Band	1 – 2 GHz	1.2 – 1.5 GHz	2 – 4 cm	Superficial and Interstitial Heating
S-Band	2 – 4 GHz	2.4 – 2.5 GHz	1 – 3 cm	Superficial Tumors, Skin Hyperthermia, Breast Hyperthermia
C-Band	4 – 8 GHz	5.8 GHz	< 1 cm	Very Superficial Lesions
X-Band	8 – 12 GHz	8 – 10 GHz	Few mm	Experimental Localized Heating

2.2. Applicators for MHT

The microwave hyperthermia applicators used for cancer treatment are generally divided into two main categories, that is, invasive and non-invasive, based on the process of delivering microwave energy to the tumor tissue [15]. Invasive applicators, also known as interstitial applicators, are placed directly inside or very close to the tumor through minor surgical procedures. Since they deliver energy directly to the affected region, they can provide precise and localized heating, making them useful for treating deep tumors. Invasive microwave hyperthermia applicators are primarily used to treat deep-seated skin tumors and lung cancer, as they enable direct, localized heating of the target tissue [16]. However, they require insertion into the body, which may cause discomfort, infection, and damage to surrounding tissues. On the other hand, non-invasive applicators deliver microwave energy externally without entering the body. Common examples include waveguides, horns, microstrip patches, and phased-array applicators. These are more suitable for superficial cancers such as skin cancer. They can effectively heat tissues near the skin surface. In addition, non-invasive systems are more comfortable for patients, easier to use repeatedly, and carry fewer clinical risks, making them a more practical choice for skin cancer treatment [17].

Figure 2 demonstrates the required parameters for an efficient microwave hyperthermia applicator. An applicator should be compact in size and low-profile, with low leakage radiation, focused near-field distribution, reduced interface reflections, and frequency-dependent specific absorption rate (SAR). The parameters are classified into electromagnetic and thermal analyses. SAR analysis evaluates the absorbed electromagnetic energy within biological tissues. It is characterized by the SAR-based penetration depth and effective field size, which indicate the depth and spatial extent of microwave energy deposition, respectively. Thermal performance is assessed using temperature distribution, hotspot minimization, selective tumor heating, thermal effective penetration depth, and thermal effective field size. Together, these parameters provide a comprehensive framework for evaluating and optimizing microwave hyperthermia applicators for safe and effective cancer treatment.

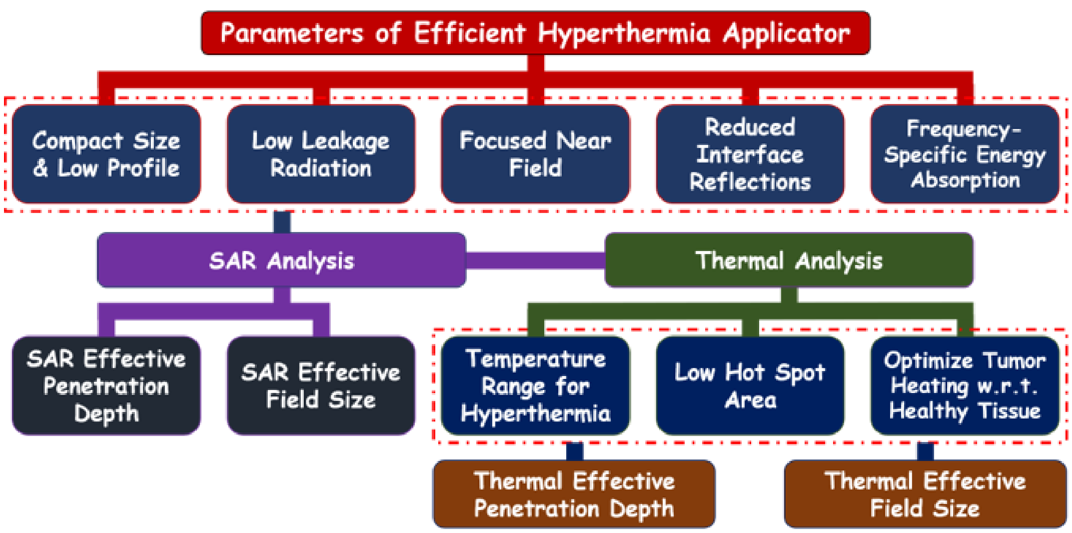

Figure 2.
Parameters for Efficient Microwave Hyperthermia Applicators.

2.3. Characterization Parameters of HT

According to the guidelines of the European Society for Hyperthermic Oncology Technical Committee, an applicator is considered effective for cancer treatment when tissue temperature increases by 6°C at a depth of 1 cm within 6 minutes. This evaluation is performed using a homogeneous phantom with muscle-equivalent electrical and thermal properties to ensure consistent performance assessment. A temperature increase of 1°C per minute corresponds to an SAR of 60 W/kg. The effective field size (EFS) is the tissue region enclosed by the 50% of maximum SAR contour measured at 1 cm depth, while EFS_{25} is identified by the 25% of maximum SAR. The distance at which the maximum SAR decreases to 13.5% is considered the penetration depth. The thermal-based effective penetration depth (TEPD) and

DOI: 10.55214/2576-8484.v10i9.13548

effective field size (TEFS) correspond to 50% of the maximum temperature rise at 1 cm depth. TEFS should be evaluated within 15 seconds to prevent healthy tissue from therapeutic damage [13].

$$APAR = \frac{P_{tumor}}{P_{healthy-tissue}} \quad (1)$$

$$TC_{25} = \frac{V_{tumor}(SAR > 0.25\ SAR_{max})}{V_{tumor}} \quad (2)$$

$$HTR = \frac{SAR\ (V_1)}{SAR_{tumor}} \quad (3)$$

$$Mean\ Tumor\ SAR = SAR_{tumor} \quad (4)$$

Where APAR = Average Power Absorption Ratio, P_{tumor} = Average Power Absorbed by Tumor, $P_{healthy-tissue}$ = Average Power Absorbed by Healthy Tissue, TC = Tumor Coverage, V_{tumor} = Tumor Volume, HTR = Hotspot-to-Tumor Ratio, V_1 = 1% of Tissue Volume.

3. Interaction of Microwaves with Biological Tissues

The interaction between microwave energy and biological tissues is primarily governed by their frequency-dependent electrical properties, including relative permittivity and conductivity. Human tissues behave as lossy dielectric materials because they contain water molecules, dissolved ions, and polar protein structures. When exposed to microwave fields, polarized molecules continuously rotate and align with the alternating electromagnetic field. This molecular motion produces displacement currents and dielectric losses because of the viscous nature of biological tissues. At the same time, free ions oscillate under the applied field, generating conduction currents and resistive energy losses. These mechanisms collectively determine the complex dielectric constant ($\varepsilon_r = \varepsilon' - j\varepsilon''$) behavior of biological tissues during microwave energy absorption. Where ε' & ε'' are the dielectric constant and loss factor of the tissue medium, respectively. The dielectric loss factor is related to conductivity by the expression ($\varepsilon'' = \sigma / \omega\varepsilon_o$), where ω is the angular frequency and ε_o is the permittivity of free space. Similarly, the loss tangent is expressed as ($tan\delta = \varepsilon'' / \varepsilon'$), indicating the electromagnetic energy dissipation capability of biological tissues. As microwave energy penetrates tissue, electromagnetic energy is converted into molecular kinetic energy, producing localized heating throughout the absorbing medium.

The heating rate depends on microwave power, operating frequency, wave polarization, tissue geometry, density, and dielectric characteristics. The absorbed electromagnetic energy is determined by SAR, which represents absorbed power per unit tissue mass. SAR (W/kg) can be calculated using equation (v). Alternatively, SAR can be estimated from the initial heating rate using equation (vi). Where |E| = total induced electric field in tissue (V/m), σ = conductivity (S/m), ρ = density (kg/m³), C = specific heat capacity (J/kg/°C), dT/dt = initial heating rate (°C/s).

$$SAR = \frac{\sigma\, |E|^2}{2\rho} \quad (5)$$

$$SAR = C\ \frac{dT}{dt} \quad (6)$$

The temperature rise predicted by this equation assumes negligible thermal conduction and blood perfusion during the initial heating period. In practical hyperthermia treatments, tissue temperature distributions are influenced by conduction, metabolism, and physiological blood circulation. Therefore, heat transfer within biological tissues is commonly modeled using Pennes' Bioheat Equation:

$$\rho C\frac{\partial T}{\partial t} = K\nabla^2 T + A_o + \rho\, SAR - B(T - T_B)$$

Where K = Muscle Thermal Conductivity (W/m/°C), A_o = Metabolic heat (W/m^3) naturally generated by body cells, B = Heat Exchange (W/m^3/°C) due to blood perfusion, T_B = Blood Temperature assumed to be constant at 37°C.

4. Antenna-based Applicators Reported for Hyperthermia Treatment of Skin & Superficial Cancer

In the 1990s, a robot-controlled microwave antenna system was designed and reported to provide uniform hyperthermia treatment for superficial tumors of arbitrary shapes, addressing a key limitation of conventional stationary applicators [18]. The authors state that standard waveguide- or microstrip-type applicators struggle to produce uniform temperature distributions over large areas, often creating a central hot spot that fails to heat the tumor periphery adequately. To achieve a therapeutic temperature (above 43°C) throughout a tumor volume while protecting healthy tissue, the authors propose a dynamic scanning system. The system utilizes a 2.45 GHz axial-mode helical antenna mounted on a six-axis robotic arm, as shown in Fig. 3. The helical antenna was selected for its compact design, small beam width, and circular polarization, which helps isolate the antenna from surface proximity effects. Movements of the robot are controlled by computer systems, which scan the antenna footprint over the disease site. The scan path determines the shape of the heating pattern, while the velocity profile controls the power deposition. The researchers used the bioheat equation to calculate ideal power distributions required for steady-state temperature uniformity. Their models for a 100 x 100 mm^2 region indicated a simulated temperature rise of 8 °C.

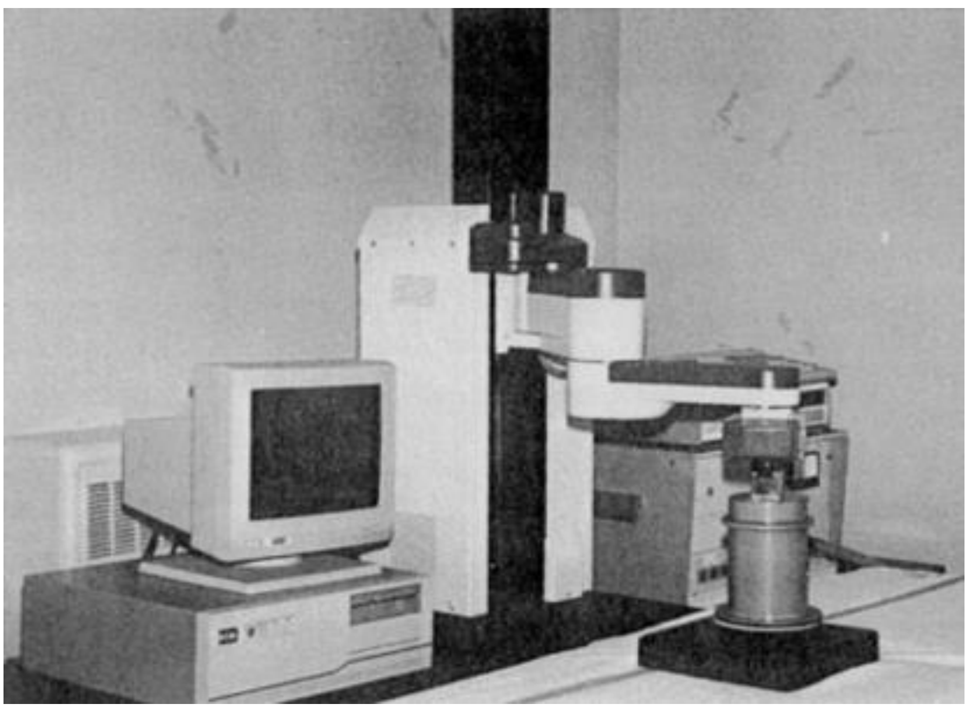

Figure 3.
UMI RTX Robot Arm with Antenna.
Source: Tennant et al. [18].

Additionally, the developed system was validated through experimental work conducted on a homogeneous muscle-equivalent phantom. The system successfully produced uniform temperature distributions over large, arbitrarily shaped areas, including squares and circles. During phantom experiments, a 30 W radiated output for 11 min produced an experimental temperature rise of approximately 10°C. The scanning system achieved uniform heating to a depth of approximately 15 mm within the muscle-equivalent phantom. The study concludes that mechanical scanning offers a viable method for achieving controlled and uniform hyperthermia. However, the authors identify several challenges for clinical implementation, such as blood perfusion, real-time feedback, and temperature monitoring.

The paper by Montecchia [19], reported in 1992, evaluates three types of microstrip patch antennas that can be used as applicators for hyperthermia treatment of superficial tumors. The authors highlight the advantages over bulky waveguide applicators due to their compact size and body-conforming nature. This research aims to address the clinical need for applicators that can treat small- to medium-sized superficial tumors located on curved body sites like the axilla or neck, where traditional waveguides are impractical. The author optimizes single-element microstrip-based antennas, specifically the microstrip disk (MDA), microstrip annular-slot (MASA), and microstrip spiral (MSPA), to achieve efficient energy delivery and uniform heating patterns. The developed MDA, MASA, and MSPA are shown in Fig. 4. MDA consists of a simple metallic patch on a low-loss dielectric substrate and is grounded by a metallic plate at the back. Testing at 150 W for 120 seconds resulted in a temperature rise of 4°C in a central hot spot. MASA is a flexible configuration of a slot antenna that utilizes resonating slots and a patch to improve radiator efficiency. It demonstrated good performance, achieving a 10°C temperature rise at a depth of 1.5 cm after just 30 seconds at 150 W. MSPA consists of a microstrip spiral antenna, which belongs to the traveling-wave antenna. It is designed for broadband operation (200–1000 MHz) with a circularly symmetric heating pattern. Furthermore, the work is validated through a test of the applicator with an equivalent phantom of homogeneous muscle, tested at a 150 W power level for 60 seconds.

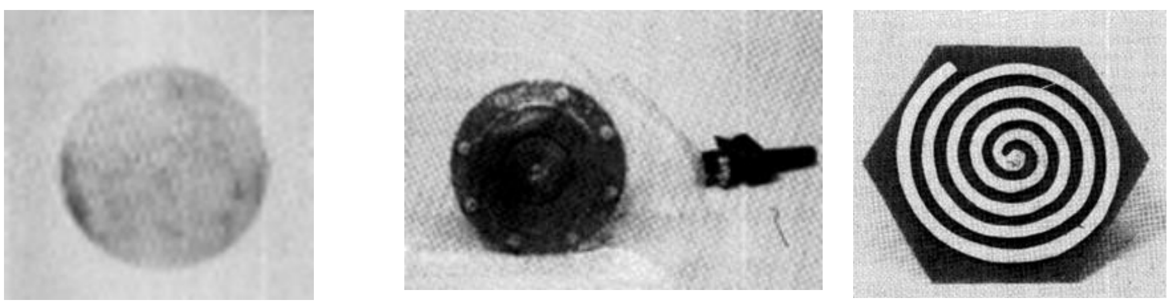

(a) (b) (c)

Figure 4.
Microstrip Applicator: (a) Disk, (b) Annular Slot, (c) Spiral.
Source: Montecchia [19].

Another paper reported in Lee et al. [20] describes the development and clinical testing of a 915 MHz microstrip array applicator specifically designed for treating large-surface-area superficial tumors. This research focuses on the clinical need for applicators that can physically conform to complex body contours. It should also provide real-time power control to adjust for tissue inhomogeneities and blood flow variations. The system uses an array of Archimedean spiral antennas as elements, as shown in Fig. 5. Each element is approximately 3.5 cm x 3.5 cm, mounted on a flexible substrate, presented in Fig. 5(a). The standard applicator utilizes a 25-element (5x5) array. The cutaway view of the array is illustrated in Fig. 5(b). A 1.5- to 4.8-cm-thick distilled-water bolus is integrated to ensure efficient coupling and provide surface temperature regulation. The 915 MHz frequency was selected to balance spatial resolution with penetration depth. It provides a half-power penetration depth of approximately 3 cm in muscle-like tissue. The developed system is powered by 100 W per-channel generators. It utilizes time-shared multiplexing with an electromechanical switch to control individual antenna elements.

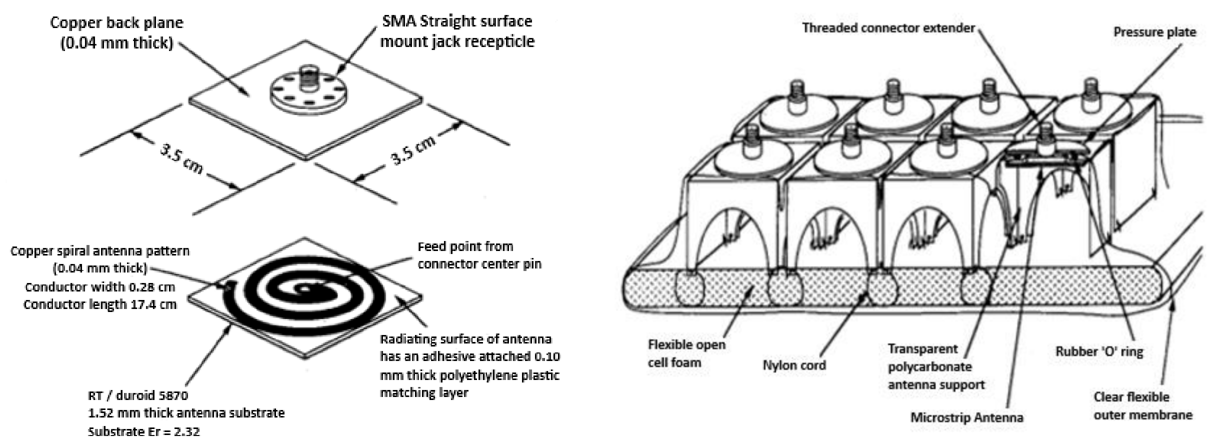

(a) (b)

Figure 5.
Microstrip Spiral Antenna: (a) Single Elements, (b) Cutaway diagram of Array.
Source: Lee et al. [20].

In the single-exposure tests, clinical heating is initiated at sufficient power to achieve a steady temperature increase of 1.5°C to 2.5°C per minute until therapeutic levels are reached. Treatments are typically maintained for up to 60 minutes. The clinically effective width of the power deposition pattern on a flat surface is 12 cm. When applied to curved surfaces, this effective width is reduced to 8 cm due to geometric effects. The developed system's design allows it to be scaled to cover large regions. However, the authors note that the main issue is the absence of high-resolution thermometry for accurate real-time optimization of power distribution over such a large array.

The paper by Cepeda et al. [21] details the design, modeling, and validation of a microcoaxial double-slot antenna specifically for interstitial hyperthermia. It provides a localized alternative to external applicators for treating tumors deep within the body. The authors address a primary limitation of external microwave applicators, such as low penetration depth in muscle tissue (0.012–0.12 m), which results in an inability to deliver uniform thermal doses to internal tumor volumes. To overcome this, they proposed a minimally invasive interstitial technique using thin antennas inserted directly into the tumor to achieve precise, local heating of 6°C to 8°C above normal body temperature. The proposed applicator presented in Fig. 6 is constructed from a UT-85 semirigid coaxial cable with two 1 mm ring slots in the outer conductor. The optimized slot spacing of 0.25λeff and 0.125λeff ensures that power is deposited specifically near the antenna slots. Validation was conducted using a muscle-equivalent phantom adjusted to a relative permittivity of approximately 52.7 and a conductivity of 1.7388 S/m. Experimental and simulation results show that the antenna could increase the local temperature by nearly 6°C using a power level of 1 W applied for 3 minutes. The effective heating field was highly localized. The thermal distribution concentrated in the region between the antenna's distal tip and the slots, covering a longitudinal area of approximately 10 mm. This precision allows for effective treatment of deep-seated tumors with minimal injury to surrounding normal tissues.

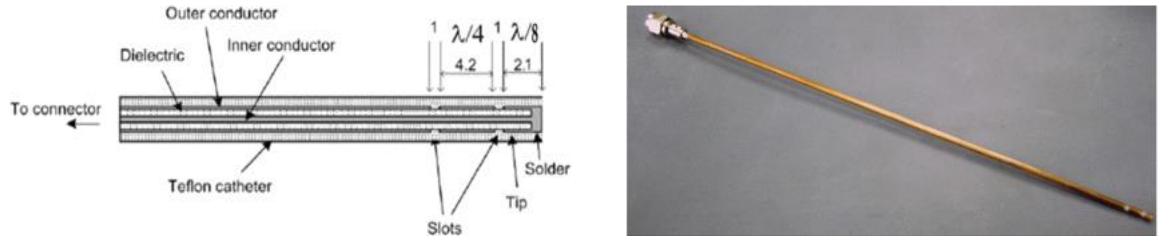

(a) (b)

Figure 6.
Coaxial-based Double Slot Antenna: (a) Proposed Applicator, (b) Prototype.
Source: Cepeda et al. [21].

The 2009 paper by Safarik and Rychlik [22] details the design, simulation, and measurement of two types of microwave planar applicators: a spiral and a slot applicator for local hyperthermia at the working frequency of 434 MHz. These planar structures were developed as a lightweight, flexible, and cost-effective alternative to bulky waveguide applicators. Using 3D electromagnetic simulators, the authors evaluated the impedance matching and specific absorption rate (SAR) distributions of these designs in a homogeneous tissue phantom. Fig. 7 presents the two different types of planar microstrip applicators. The spiral applicator shown in Fig. 7(a) features a metallic Archimedean spiral that radiates circular polarization and is specifically designed to eliminate hotspots during treatment. One of its primary advantages is its wideband nature, which ensures that the working frequency remains stable despite variations in the dielectric constant of the targeted tissue. In contrast, the slot applicator illustrated in Fig. 7(b) is a resonant structure where the slot circumference corresponds to approximately one wavelength. While this design is more sensitive to tissue dielectric properties, the authors found that this dependence can be effectively managed by using a water bolus. Experimental results, validated via thermographic measurements, showed a high level of agreement with the simulations. The slot applicator was found to provide a larger effective field size (EFS) compared to the spiral design, though both applicators are capable of treating superficial areas approximately 3–4 cm in diameter. The study concludes that both planar designs are suitable for superficial hyperthermia, with the spiral applicator being ideal for cases requiring high bandwidth stability and the slot applicator being preferable for heating larger areas.

ISSN: 2576-8484
Vol. 10, No. 9: 21-53, 2026
DOI: 10.55214/2576-8484.v10i9.13548

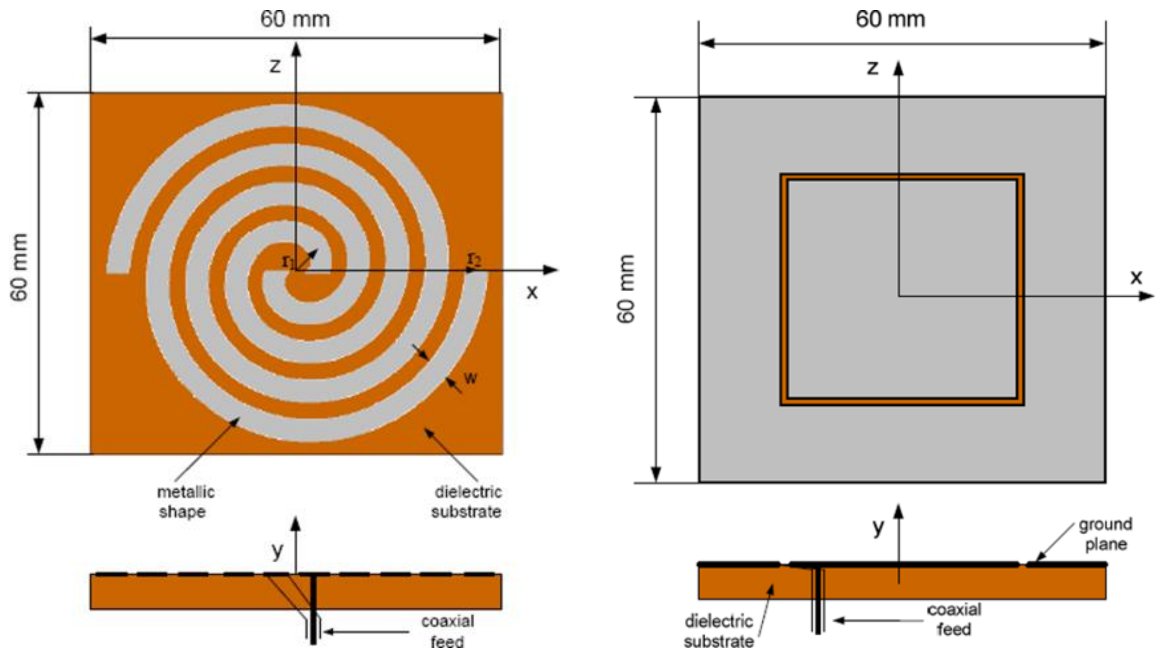

(a) (b)

Figure 7.
Planar Microstrip Applicator: (a) Spiral, (b) Slot.
Source: Safarik and Rychlik [22].

The 2012 paper by Koo et al. [23] describes a conformal, flexible microstrip antenna design shown in Fig. 8. It operates at 434 MHz for treating superficial skin cancer. The applicator uses elastic silicone layers and very bendable, thin substrates. The total size of this antenna is 150 mm x 110 mm. It contains five layers, including three silicone pads and two substrates, as presented in Fig. 8(a). Figs. 8(b) and 8(c) illustrate the top view and fabricated prototype, respectively. Layer one acts as a buffer to prevent direct skin contact. Simulation shows a penetration depth reaching up to 46.2 mm. The effective field size for this specific design is 75 cm^2. The calculated effective heating depth for the tissue is 14.1 mm. Clinical trials involved veterinary patients (dogs). The system achieved a very wide measured impedance bandwidth of 400 MHz. This design effectively avoids air gaps due to its flexibility and provides uniform heat distribution.

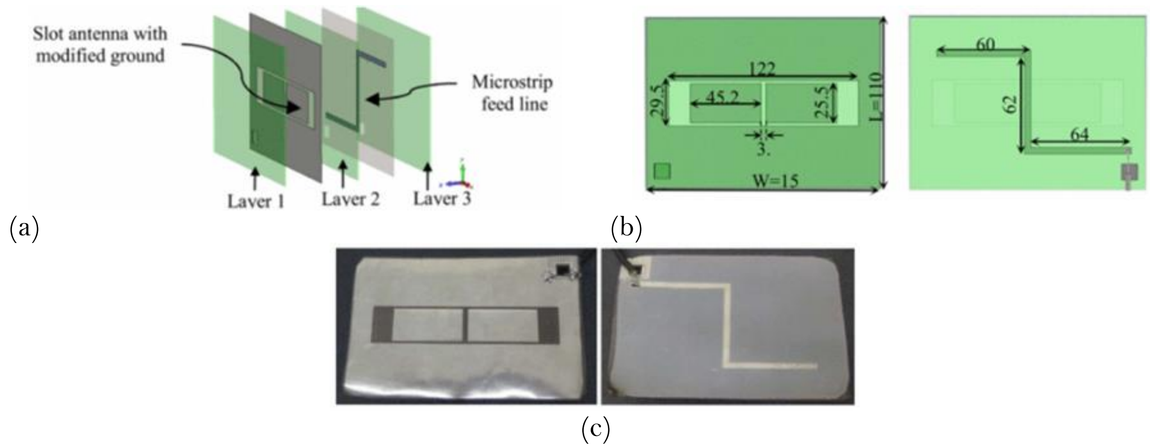

Figure 8.
Conformal Flexible Antenna: (a) Prospective View, (b) Top View, (c) Fabricated Prototype.
Source: Koo et al. [23].

Petrishia and Sasikala [24] describe a prolate-spheroidal impulse-radiating antenna. The antenna design presented in Fig. 9 utilizes tapered arms to enhance antenna gain for skin cancer treatment. The system targets melanoma cells using non-invasive, ultra-short electrical pulses. These high-voltage pulses have a duration of only 100 picoseconds. Additionally, a ten-layer log-periodic lens is introduced to decrease the spot size and match the 100-picosecond pulses to a skin phantom. This lens system increases the focal electric-field intensity significantly. The electric-field amplitude rises from 52.9 V/m to 91.29 V/m at the focal point. Furthermore, the peak electric field reaches 114 V/m in the presence of a tumor. The effective focal spot size is reduced from 1 cm to 0.75 cm. This reduction minimizes damage to healthy tissue layers surrounding the target. In contrast to traditional hyperthermia, this method uses electrical impulses to induce apoptosis. Consequently, the paper focuses on pulse intensity rather than a slow temperature rise. Figures 8(a) and 7(b) illustrate the side view and cross-sectional view of the lens-based antenna, respectively.

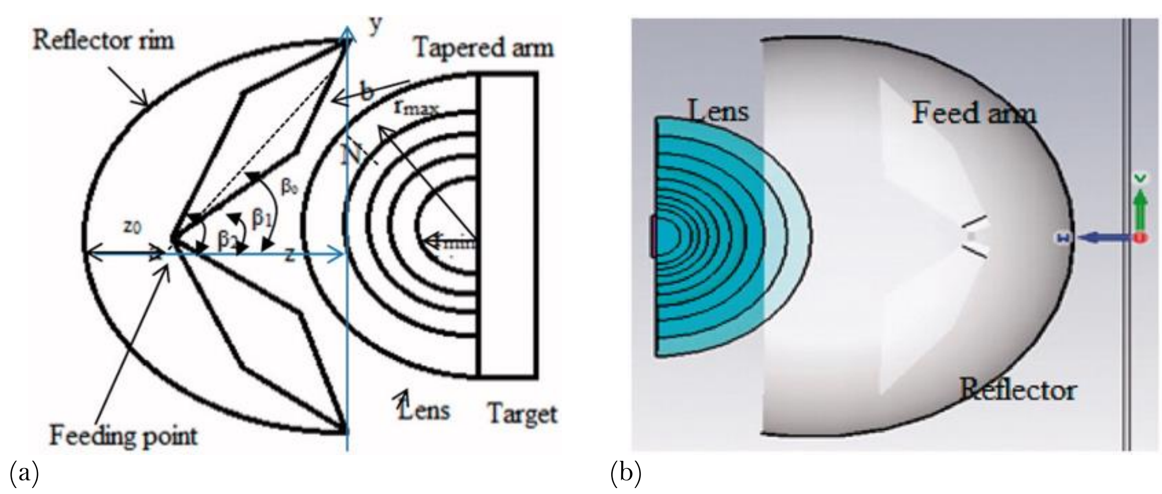

Figure 9.
Lens-based Prolate Spheroidal Impulse Radiating Antenna: (a) Side View, (b) Cross Section View.
Source: Petrishia and Sasikala [24].

Chakaravarthi and Arunachalam [25] describe the design and characterization of a miniaturized 434 MHz cavity-backed patch antenna. The evolution steps of the antenna are shown in Fig. 10, where Fig. 10(A) represents the simple rectangular microstrip antenna. The C-type folded patch with and without shorting pins is presented in Fig. 10(B) and 10(C), respectively. The primary goal was to create a compact applicator with stable resonance less affected by changing tissue loads or the environment. Miniaturization was achieved through dielectric loading, a metal enclosure, a folded patch design, and an integrated shorting post. This exceptionally compact device features a tiny patch housed inside a small metal cavity measuring 40 x 12 mm². An integrated 35 mm coupling water bolus serves to cool the skin surface and improve electromagnetic coupling with tissue. The authors delivered high-power microwave pulses to muscle-equivalent phantoms and then measured the results using an infrared thermal camera for characterization. This research utilized short pulses to calculate the Specific Absorption Rate instead of focusing on traditional long-term therapeutic maintenance protocols. The fabricated prototypes are shown in Fig. 11. The C-type folded patch with shorting pins, with a 0.3 mm thick flexible PVC water bolus, a rigid side-wall bolus, and flexible PVC on the skin-contact side are illustrated in Fig. 11(A), 11(B), and 11(C), respectively. Applying a pulse of 24 W for 60 seconds resulted in a temperature rise of 2.33°C. When the duration of the pulse was extended to 90 seconds, the temperature rise reached 3.29°C in the muscle phantom of polyacrylamide.

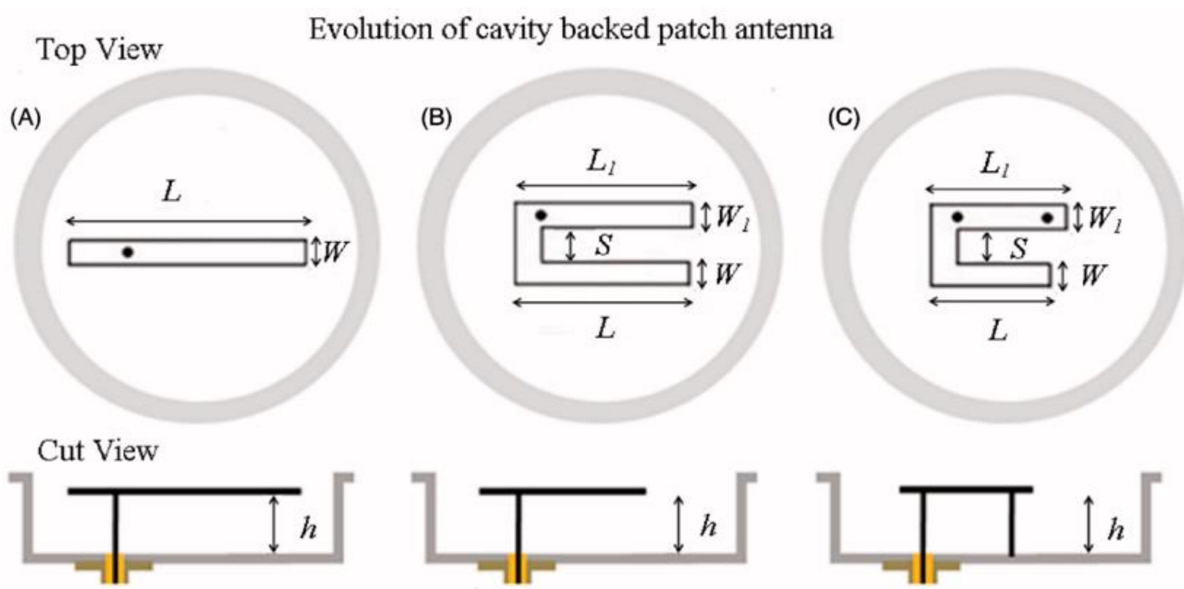

Figure 10.
Cavity-Backed Patch Antenna Evolution: (A) Rectangular Patch, (B) C-type Folded Patch, (C) C-type Folded Patch with Shorting Pins.
Source: Chakaravarthi and Arunachalam [25].

Further experiments using a 26 W pulse on gelatin phantoms resulted in a much higher temperature rise of 5°C. Experimental testing confirmed a -3 dB SAR penetration depth of 8.25 mm, which closely aligns with the simulations. Simulation data indicated a SAR coverage of 3.09 cm² along the depth of the phantom, while physical measurements showed a coverage area of 3.21 cm². At a depth of 5 mm, physical testing confirmed a lateral heating width of 49.47 mm across the surface. The miniaturized applicator is suitable for superficial cancer treatment and also enables effective heating of deep-seated tumors.

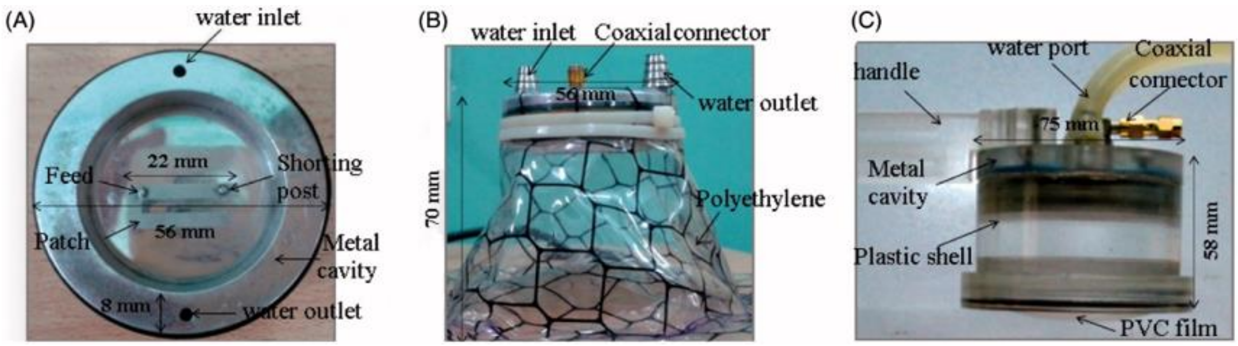

Figure 11.
Fabricated Prototypes: (A) Fabricated C-type Folded Patch with Shorting Pins, (B) with 0.3 mm thick Flexible PVC Water Bolus, (C) Rigid Side Wall Bolus and Flexible PVC in Skin Contact Side.
Source: Chakaravarthi and Arunachalam [25].

A Singh and Singh [26] describe a microstrip slot antenna designed for superficial microwave hyperthermia applications. This compact applicator measures 29 x 29 mm² and utilizes a simple 50 Ω microstrip line to excite the antenna. Its unique geometry consists of two circular conducting patches enclosed within a rectangular slot on a modified ground plane, as presented in Fig. 12. The simulations revealed a high penetration depth of 23 mm and a significant bandwidth of 170 MHz. The antenna maintains stable resonance at 2.45 GHz even when the dielectric properties of muscle tissue change. Compared to traditional patch designs, this slot antenna provides better resolution and more uniform power distribution across the target. The optimized geometry shown in Fig. 12(a) produces an effective field size of 12 x 18 mm² at the tumor depth. Fig. 12(b) shows the proposed antenna placed with a phantom. This research concludes that the proposed slot configuration is a better choice for heating localized superficial tumors during treatment.

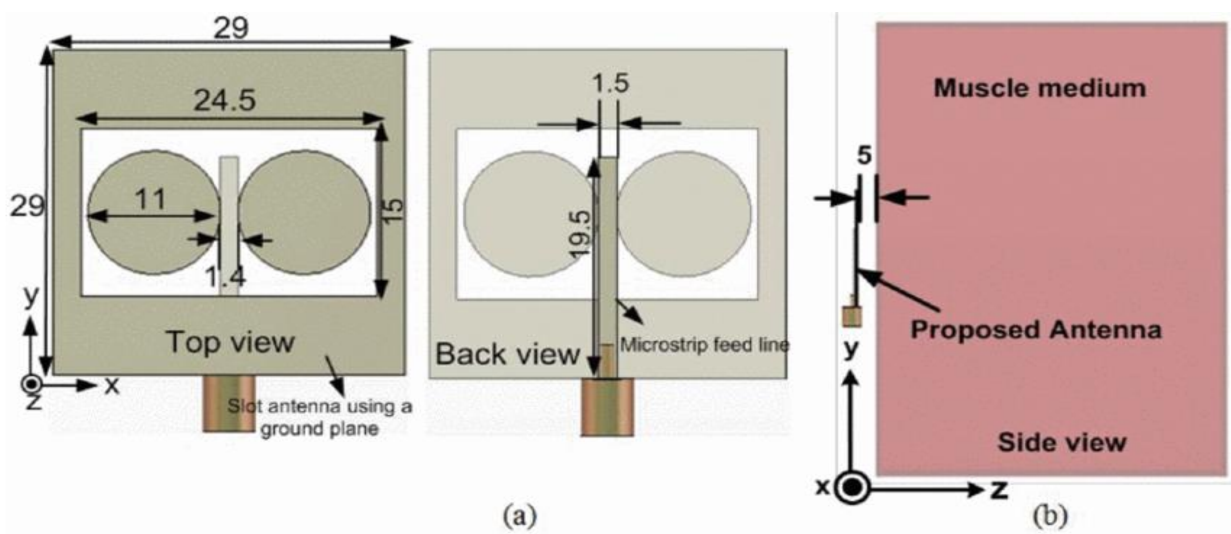

Figure 12.
Microstrip Slot Antenna: (a) Proposed Geometry, (b) Proposed Antenna with Phantom.
Source: Singh and Singh [26].

Another study by Singh and Singh [27] reported a water-loaded metal-dielectric wall diagonal horn antenna for hyperthermia application. The water-loaded diagonal horn antenna is illustrated in Fig. 13. This specialized applicator operates at 2.45 GHz to heat cancerous tumors located within the human body. The design incorporated Lucite dielectric walls combined with metal portions to improve field distribution and penetration depth. Filling the horn with deionized water ensures a stable impedance match between the antenna and the muscle medium. Simulations revealed a significant penetration depth of 20.3 mm when the energy is delivered into a muscle phantom. The simulated effective field size of 17 x 17 mm² exhibits a symmetric field distribution at tumor depth. The antenna generates a peak SAR value of 154 W/kg at an excitation power of 2 W. The thermal simulation was initiated with a baseline body temperature of 37°C. The antenna raised the muscle temperature to approximately 52°C at the surface and 46°C at a depth of 10 mm. The proposed antenna is suitable for both superficial and deep-seated cancer treatment by providing effective heating at surface and subsurface tissue depths.

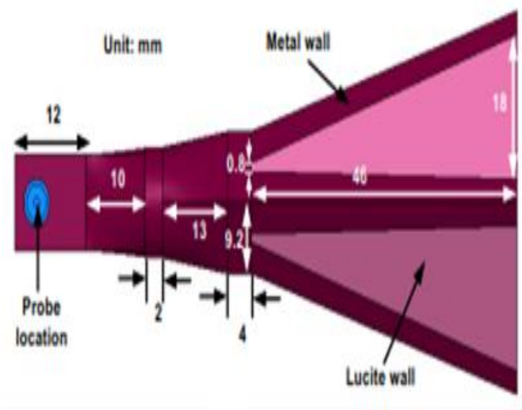

(a)

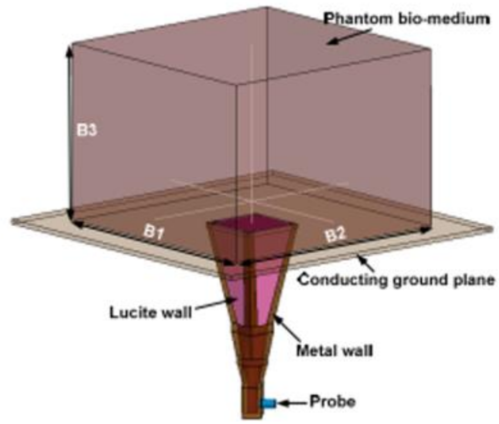

(b)

Figure 13.
Water-Loaded Diagonal Horn Antenna.
Source: Singh and Singh [27].

The authors Kim et al. [28] propose a planar 8x8 array for non-invasive local hyperthermia. This specialized applicator, shown in Fig. 14, operates at 915 MHz to treat tumors at various depths beneath the skin. The unit cell of the phased-array applicator is presented in Fig. 14(a). A lattice-array configuration shown in Fig. 14(b) can be used with or without advanced phased-feeding techniques. The applicator produces localized heating in the near-surface region when all elements are excited with identical phases, enabling effective treatment of superficial tumors. The 8x8 lattice array is excited with an input power of 1.125 W per element for 60 minutes. The resulting temperature distribution covers 61% of the 158 x 158 mm² phantom aperture at a depth of 20 mm below the skin surface. Phased feeding enables the system to focus microwave energy at greater depths, facilitating ultra-superficial hyperthermia treatment. This technique increases the simulated effective heating depth from 36 mm to 49 mm in the phantom. For enhanced penetration, each array element operates at a reduced input power of 0.345 W for 60 minutes. To prevent excessive skin heating while concentrating energy on deeper targets, a circulating ice-water bolus is employed during treatment.

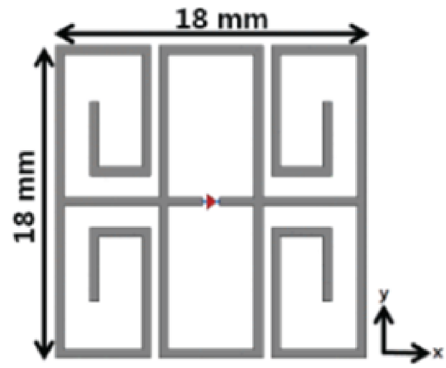

(a)

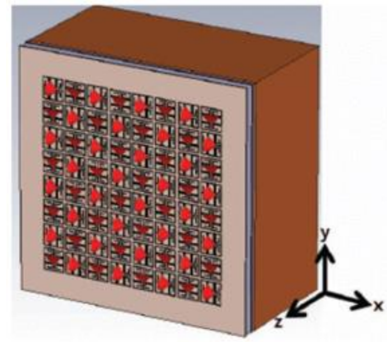

(b)

Figure 14.
Phased Array Applicator: (a) Unit Cell, (b) 8x8 Array.
Source: Kim et al. [28].

The researchers developed a dual-band antenna [29] operating at 434 MHz and 915 MHz for superficial local hyperthermia in 2017. The antenna excites the TM_{01} mode at the lower frequency and the TM_{21} mode at the higher frequency. Fig. 15 shows the proposed square-ring microstrip patch antenna. As illustrated in Fig. 15(a), the proposed geometry comprises a square ring incorporating an internal square patch on an FR-4 substrate. This compact antenna has a total volume of 124 x 124 x 1.6 mm^3 for better clinical usability. The design includes a slotted ground plane, as depicted in Fig. 15(b), and a metallic via to adjust the resonance frequencies and improve performance. HFSS software is used to optimize the geometric parameters, the feeding port, and the specific via position. A planar trilayered tissue model containing skin, fat, and muscle, with a water bolus layer, was employed to simulate the biological effects. The antenna achieves penetration depths of 6 cm at 434 MHz and 6.5 cm at 915 MHz inside phantom tissues. For an input power of 1 W, the maximum SAR values obtained are 1.32 W/kg and 1.44 W/kg at the lower and higher frequency bands, respectively.

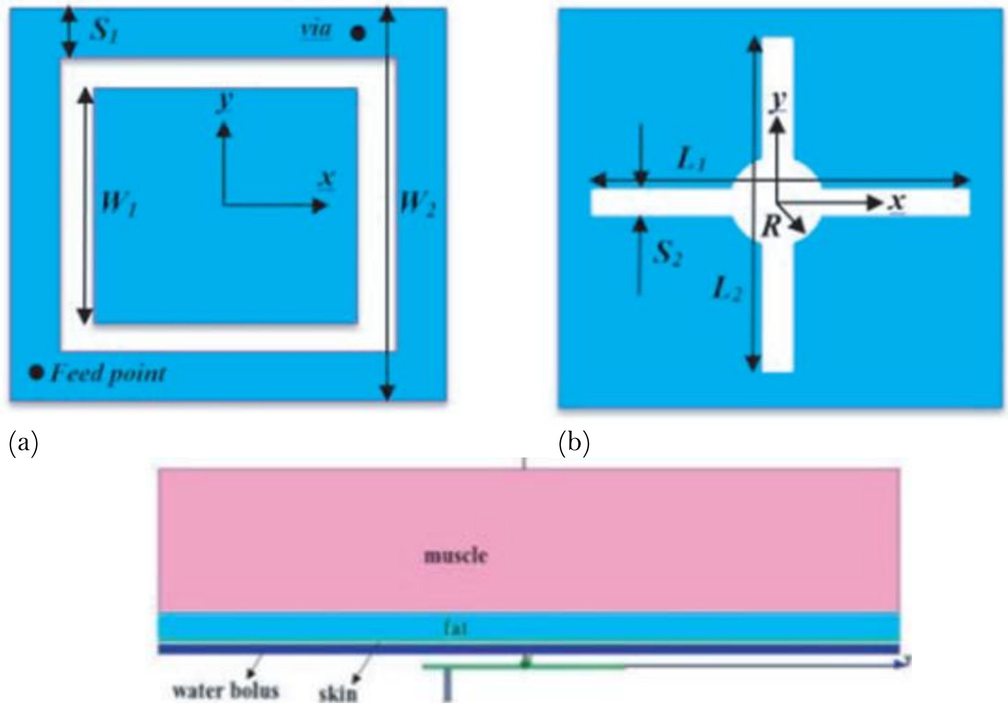

(a) (b)

(c)

Figure 15.
Square Ring Microstrip Patch Antenna: (a) Front side Patch, (b) Back side Ground, (c) Antenna placed with Tri-layered Phantom and Water Bolus.
Source: Younesiraad et al. [29].

A miniaturized lens-based prolate spheroidal impulse radiating antenna (PSIRA) [30], presented in Fig. 16, was proposed in 2018 for non-invasive skin cancer therapy. The applicator consists of a prolate spheroidal reflector. The excitation is provided by a modified bicone antenna illustrated in Fig. 16(a), positioned at the first focus of the reflector. A three-layered dielectric lens is integrated to enhance the spatial resolution on the targeted biological skin tissue, as depicted in Fig. 16(b). The antenna operates over a wide frequency spectrum from 2 GHz to 30 GHz to accommodate extremely fast pulses. This specific frequency range was selected to deliver 100-picosecond pulses capable of permeabilizing the membranes of cancer cells. Researchers modeled the target using a two-layer skin phantom comprising the epidermis and dermis, with specific dielectric properties. The applicator focuses the intense electric pulse generated at the first focal point onto the second focal point, where the phantom is placed. The second focal point is located 186 mm from the reflector vertex. Using the lens, the effective spot size is significantly reduced to 6 mm in the lateral direction and 3 mm in the axial direction, thereby minimizing potential damage to healthy surrounding tissues. The enhanced electric-field peak at the focus reached 294 V/m with a 1 V input signal. This research focuses on a non-thermal therapy approach for skin cancer that induces cell death using an intense pulsed electric field.

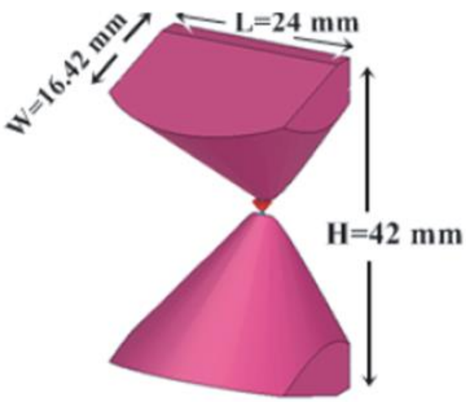

(a)

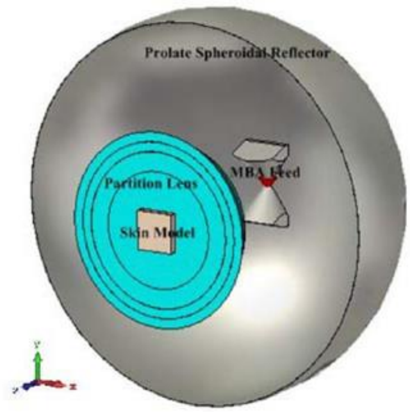

(b)

Figure 16.
Lens-based Prolate Spheroidal Impulse Radiating Antenna: (a) Bicone Antenna, (b) Bicone Antenna with Prolate Spheroidal Reflector and Lens.
Source: Petrishia [30].

The researchers designed a compact rectangular patch antenna [31] with overall dimensions of 30x30 mm^2 in 2022. This design features a rectangular spiral structure to ensure efficient radiation for local hyperthermia therapy, as shown in Fig. 17. The methodology involves utilizing simulation software to analyze the antenna's return loss and radiation pattern characteristics. Investigators aimed to create a miniaturized applicator suitable for high directivity and portable hyperthermia clinical systems. The proposed antenna operates within frequencies spanning from 0.6 GHz to 0.8 GHz. It achieves a resonance peak at 0.6812 GHz with a simulated return loss of 26.38 dB. This frequency range was specifically selected to facilitate low-frequency operation. The antenna exhibits a directivity of 2 dB, which focuses most radiated energy toward the targeted broadside treatment region. Such capabilities allow the antenna to target malignant cells effectively through concentrated electromagnetic radiation delivery. Simulation results indicate that energy distribution is concentrated specifically at the point where localized heating is required.

DOI: 10.55214/2576-8484.v10i9.13548

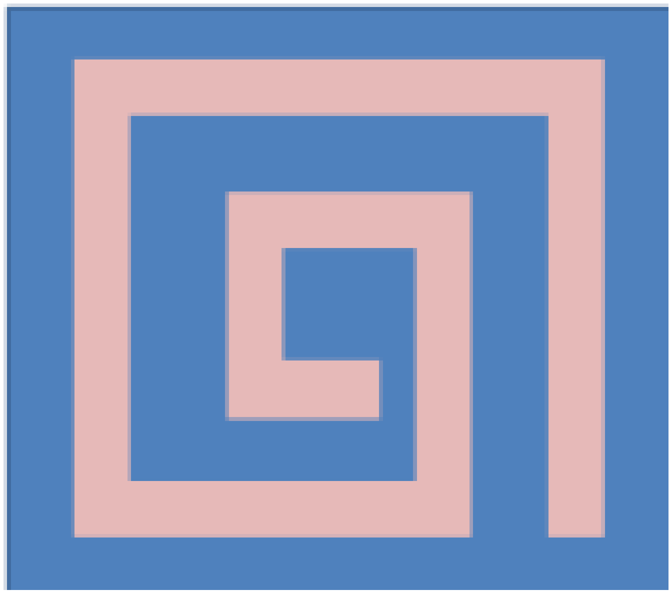

Figure 17.
Rectangular Spiral Patch Antenna.
Source: Tyagi et al. [31].

The paper presented in Kaur and Kaur [32] reports an advanced Archimedean spiral microwave hyperthermia applicator in 2023. The applicator employs a compact 38 x 38 mm^2 spiral patch antenna, as illustrated in Fig. 18, fabricated on a 1.57 mm-thick FR-4 substrate. The antenna consists of a single three-turn spiral resonator designed to achieve efficient electromagnetic energy delivery for hyperthermia treatment. To enhance the front-to-back ratio and improve energy confinement, the spiral antenna is backed by a 48 x 48 mm^2 artificial magnetic conductor (AMC) reflector, as shown in Fig. 19(a). The corresponding unit cell of the AMC reflector is presented in Fig. 19(b). The applicator operates at 2.45 GHz within the ISM band and provides an impedance bandwidth of 170 MHz. Its performance was evaluated using a trilayer biological phantom comprising skin, fat, and muscle tissues. The proposed applicator achieves a peak SAR of 8 W/kg, ensuring safe and concentrated heating of targeted malignant cells. A penetration depth of 29.5 mm inside the trilayer skin phantom is observed. It demonstrates an effective field size of 36 × 36 mm^2, enabling the treatment of both superficial and moderately deep tumors. Thermal analysis based on Pennes' bioheat equation demonstrates a maximum temperature rise of 45 °C within 30 minutes. Experimental validation using a semisolid tissue-mimicking phantom confirms the therapeutic heating performance after 45 minutes of continuous microwave exposure. The AMC-backed configuration effectively concentrates electromagnetic energy within the target region while minimizing undesired heating of the surrounding healthy tissues.

ISSN: 2576-8484
Vol. 10, No. 9: 21-53, 2026
DOI: 10.55214/2576-8484.v10i9.13548

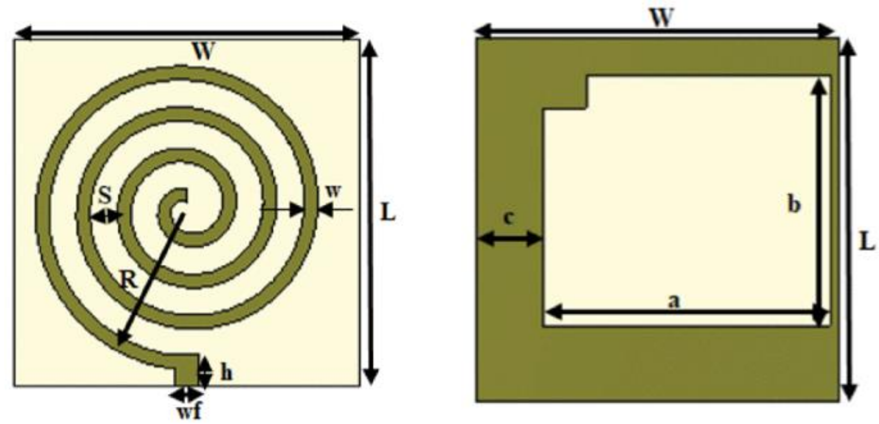

(a) (b)

Figure 18.
Spiral Antenna: (a) Top View, (b) Bottom View.
Source: Kaur and Kaur [32].

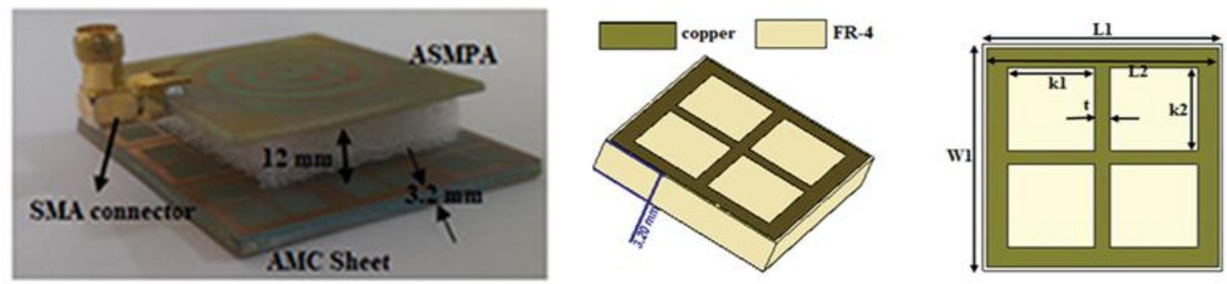

(a) (b)

Figure 19.
Applicator: (a) AMC-backed spiral applicator, (b) AMC Unit Cell.
Source: Kaur and Kaur [32].

The 2023 research Khan et al. [33] presents a compact dual-band star patch antenna as shown in Fig. 20. A compact dual-band antenna features a total volume of 26 x 26 x 1.6 mm^3. Its geometry involves a star patch integrated with four rectangular strips and shorting pins on an FR-4 substrate. Researchers utilized the high-frequency structure simulator (HFSS) software based on the finite element method for optimizing the design parameters. Two specific ISM bands at 2.45 and 5.35 GHz were selected for hyperthermia. These frequencies target malignancies located in the head and neck regions by efficiently absorbing radiofrequency power in tissues. Performance analysis involved both single-layered and multi-layered tissue-equivalent phantoms containing skin, fat, and muscle layers. The reflection coefficient achieved values of -16 dB and -19 dB at the respective operating frequencies. Simulated results for SAR reached 254 W/kg at the first resonance, and at the higher resonance, SAR reached 2041 W/kg.

ISSN: 2576-8484
Vol. 10, No. 9: 21-53, 2026
DOI: 10.55214/2576-8484.v10i9.13548

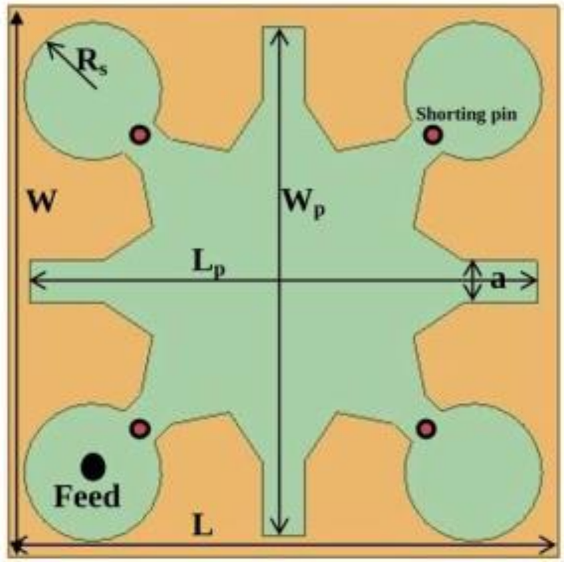

Figure 20.
Compact Dual-band Star Shape Patch Antenna.
Source: Khan et al. [33].

Gu et al. [34] present a compact dual-mode split-ring resonator (SRR) applicator array in 2023, which is depicted in Fig. 21. The stack-up layer and geometry of the proposed sensor or applicator are shown in Figs. 19(a) and 19(b), respectively. This compact applicator system features a 3x3 unit-cell array fabricated on a multilayer FR-4 substrate. Each unit cell contains rectangular split-ring resonators with capacitively loaded bars to enhance resonance and sensing sensitivity. The authors included fences around the resonators and transmission lines to provide the necessary electric-field shielding for performance. The isolation substrate thickness measures 0.2 mm, while each sensing unit's width is 3.8 mm. The applicator operates across a wide frequency range of 8–15 GHz for higher resolution. These frequencies were selected to improve the sensing resolution needed to detect and treat actual skin cancer lesions. Intense electric fields are highly focused and concentrated across the split-ring-resonator gap to target cancerous tissue. Thermal verification using chicken breast demonstrated a significant temperature rise of 15°C during testing. This thermal increase was achieved within only 180 seconds using 5 W of total power.

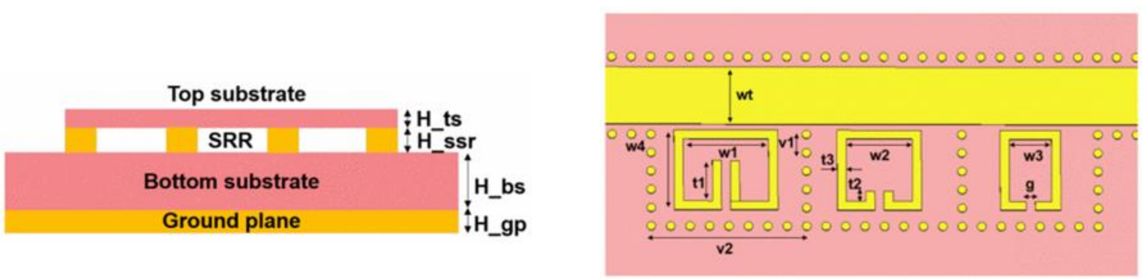

(a) (b)

Figure 21.
Proposed Sensor / Applicator: (a) Stack-up Layer, (b) Geometry.
Source: Gu et al. [34].

A circular ring microwave applicator [35], as shown in Fig. 22, was proposed by the author in 2023. This compact geometry consists of concentric annular rings fabricated on a Rogers RO3010

Edelweiss Applied Science and Technology
ISSN: 2576-8484
Vol. 10, No. 9: 21-53, 2026
DOI: 10.55214/2576-8484.v10i9.13548

substrate with cavity-backing pins. The top layer includes three rings with different radii, starting from 20 mm down to 6 mm with 1 mm spacing. The authors utilized a slotted ground plane featuring meander-line slots to achieve miniaturization and improve the impedance-matching properties. The antenna operates at 434 MHz to treat superficial cancers extending 3 cm from the skin surface. Simulation analysis involved homogeneous muscle models and heterogeneous patient models derived from magnetic resonance imaging and segmentation data. The applicator achieves a significant penetration depth of 13.67 mm while providing high power-coupling efficiency. This design provides an effective absorption-rate coverage of 18 cm^2 at a depth of 5 mm. Peak SAR values reach 417 W/kg at 5 mm depth using 26 W. The assessment of patient-derived phantom models indicates that the proposed applicator is suitable for localized superficial hyperthermia treatment.

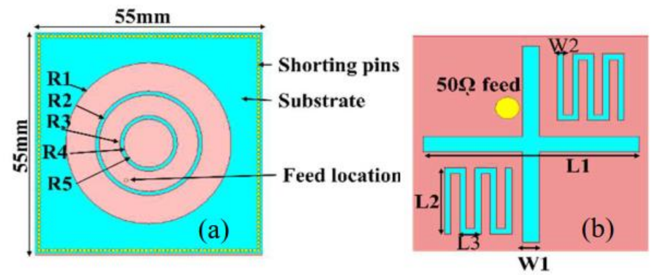

Figure 22.
Ring Antenna: (a) Top View, (b) Bottom View.
Source: Alex and Chakaravarthi [35].

In the 2024 study, a compact hybrid fractal microstrip patch antenna (HFMPA) is reported by Kaur et al. [36] and illustrated in Fig. 23. This hyperthermia applicator utilizes a hybrid fractal antenna, a metamaterial reflector, and an electromagnetic lens to treat superficial skin cancer non-invasively. A hybrid fractal patch measuring 30 × 26 mm^2 is fabricated on a Rogers RT5880 substrate. The system operates at 2.45 GHz within the designated ISM band for medical hyperthermia applications. The observed −10 dB bandwidth is 190 MHz, ranging from 2.35–2.54 GHz. This specific frequency choice ensures efficient energy absorption while minimizing potential damage to surrounding healthy biological tissues. Integration of the electromagnetic lens significantly reduces the beam width to 50° for higher power concentration levels. Although penetration depth has improved, the effective temperature area is measured as 36 × 20 mm^2. A prospective view of the microwave hyperthermia applicator is shown in Fig. 23(a), while Fig. 23(b), Fig. 23(c), and Fig. 23(d) present the HFMPA, AMC reflector, and EM lens, respectively. Thermal analysis indicates a temperature rise to 44°C after 45 minutes of exposure. Furthermore, experimental results showed that this therapeutic temperature threshold was achieved after 22 minutes of continuous microwave radiation at target sites. A reported absorption rate of 10 W/kg ensures clinical efficacy while maintaining safety standards for patients.

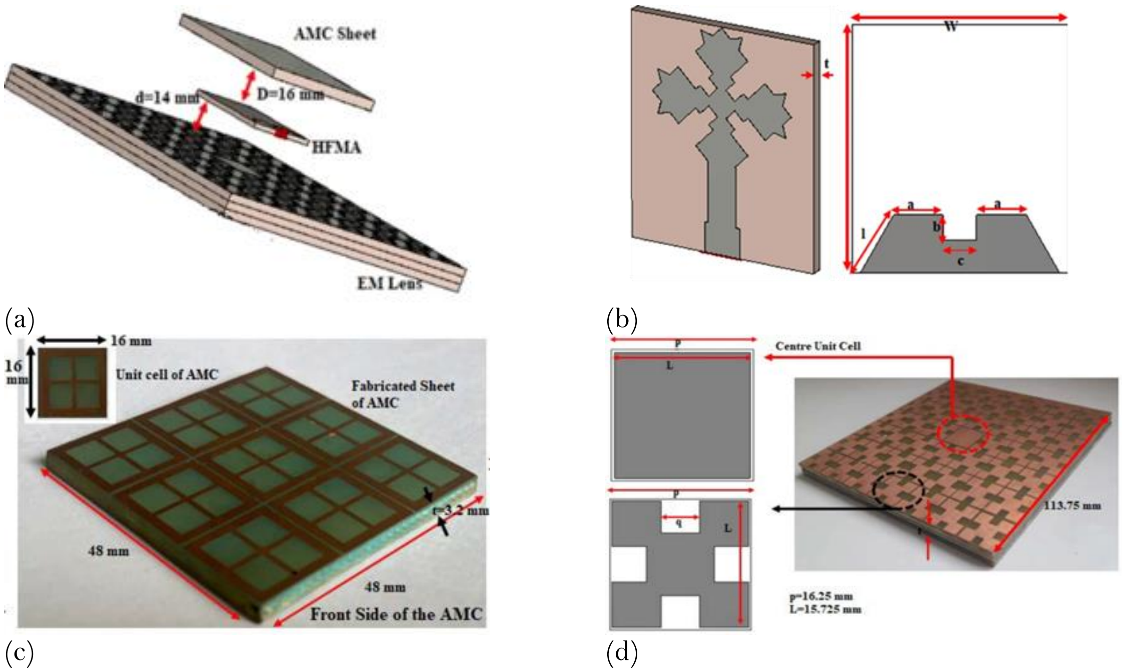

Figure 23.
Microwave Hyperthermia Applicator: (a) Prospective View, (b) HFMPA, (c) AMC Reflector, (d) EM Lens.
Source: Kaur et al. [36].

The researchers present a compact modified double-folded dipole antenna [37], as depicted in Fig. 24, in 2024. This applicator is fabricated on a Rogers 3003 substrate and features overall dimensions of 25 x 25 x 30 mm^3. The design utilizes a PETG three-dimensional-printed structure for rigidity and an RG-58 coaxial cable for ground connections. Researchers used a software-defined radio and power amplifier to deliver four watts of output power during testing. The antenna operates at 2.45 GHz, which is a standard frequency for superficial microwave hyperthermia treatments. Experimental validation was performed on a spherical skin-mimicking phantom that reflects dielectric properties defined in the current IEEE standard requirements. The system generates an almost circular thermal footprint with a diameter of 3 cm, suitable for typical melanoma lesions. A temperature increase of 17°C was achieved after a continuous application time of only 10 minutes. The applicator provides effective power deposition for superficial cancers while maintaining a very small footprint on the targeted tissue. This lightweight design ensures robust manufacturing and eliminates the need for water boluses during local hyperthermia therapy sessions.

Edelweiss Applied Science and Technology
ISSN: 2576-8484
Vol. 10, No. 9: 21-53, 2026
DOI: 10.55214/2576-8484.v10i9.13548

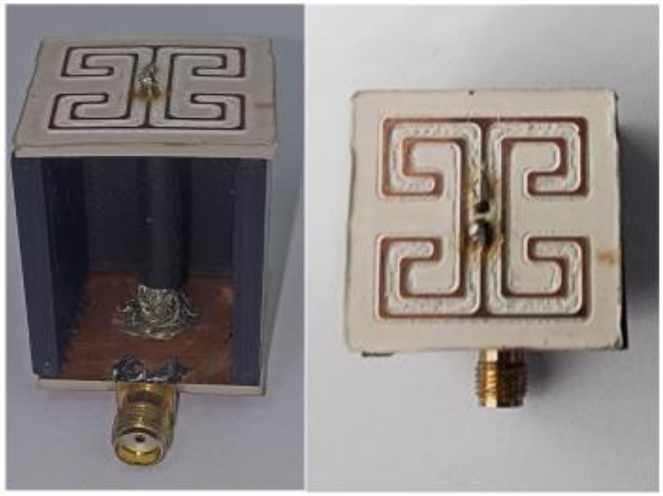

Figure 24.
Folded Dipole Applicator.
Source: Duque et al. [37].

The paper by Kaur et al. [38] presents a compact double-spiral antenna specifically designed for hyperthermia treatment of skin and neck cancers, illustrated in Fig. 25. The antenna dimensions are 31.5 mm x 31.5 mm x 0.27 mm, enabling a compact and lightweight structure. A flexible polyethylene terephthalate (PET) substrate was employed to provide mechanical flexibility and compatibility with biological tissues. The design incorporates aperture coupling and a defected ground structure (DGS) to enhance impedance matching and efficient power delivery. The applicator operates at 915 MHz within the ISM band for targeting superficial and deep malignancies. A bandwidth of 9.98 MHz is observed, ranging from 912.56 to 922.54 MHz. Investigations involved detailed simulation studies conducted under open boundary conditions, along with a tissue-mimicking phantom and the Gustav human model. This specific frequency was selected to improve power absorption and ensure a more uniform temperature distribution inside tissue. SAR analysis demonstrates a peak value of 8 W/kg in the target region. The proposed antenna applicator achieves a penetration depth of 20 mm when energized with only one watt of input power.

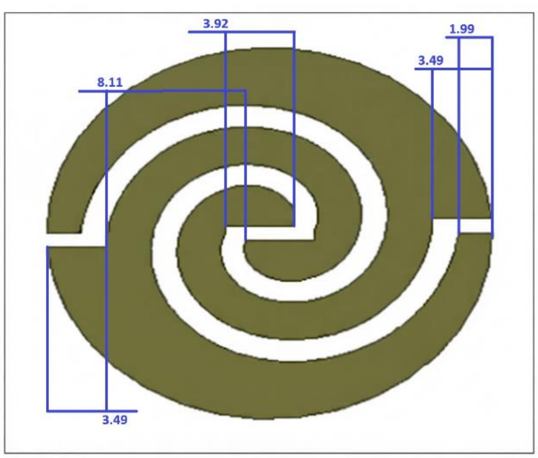

(a)

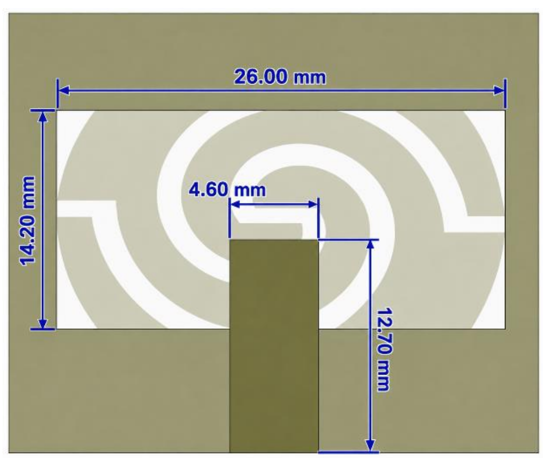

(b)

Figure 25.
Dual Spiral Antenna: (a) Top View, (b) Bottom View.
Source: Kaur et al. [38].

Another research study reported in 2025 presents a microstrip slotted antenna [39] with dimensions of 110 x 110 x 1.6 mm^3. The applicator geometry, consisting of four C-shaped and four T-shaped slots mirrored in all four quadrants of the patch, is depicted in Fig. 26. An applicator is developed on an FR-4 substrate having a dielectric constant of 4.4. This design utilizes a 50-ohm coaxial feed to excite the antenna structure at the specific resonance of 915 MHz. Simulations are performed with a single-layer tissue-equivalent phantom and a three-layer biological phantom model. An observed SAR of 169.84 W/kg was achieved at a penetration depth of 2 millimeters.

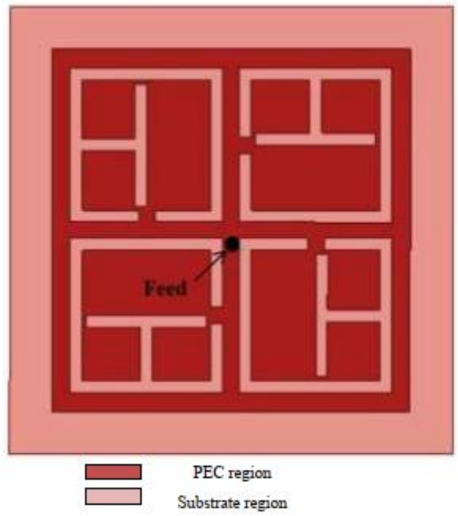

Figure 26.
Microstrip Slotted Antenna.
Source: Khan et al. [39].

The authors proposed a compact water-loaded 434 MHz antenna [40] for treating localized superficial cancers in 2025. The geometry consists of a miniaturized folded patch antenna encapsulated within a cavity-backed structure using a distilled-water substrate, as shown in Fig. 27. The final design features a small aperture area of 13.68 cm^2 for improved power-coupling stability. The chosen operating frequency of 434 MHz allows deeper therapeutic penetration than standard 915 MHz hyperthermia systems. This frequency specifically targets superficial cancers extending up to 3 cm from the contoured surface of the human body.

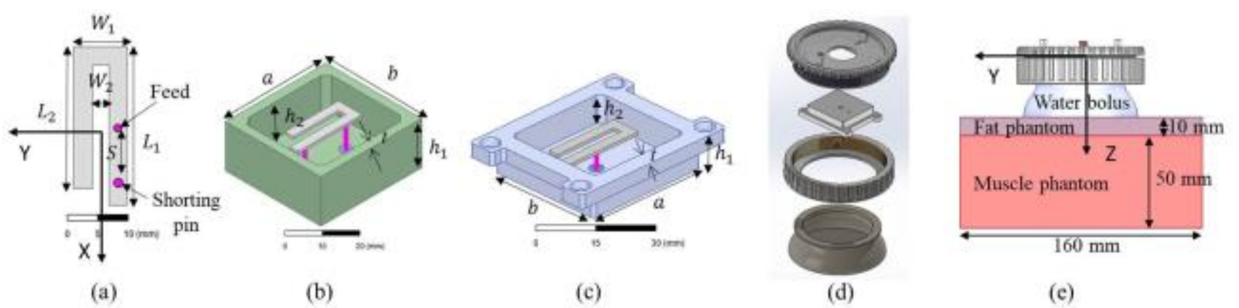

Figure 27.
Water-Loaded Antenna Applicator: (a) Folded Patch, (b) & (c) Cavity-Backed Folded Patch, (d) Applicator Internal Assembly, (e) 3D Model of Applicator with Layer Phantom.
Source: Choudhary and Arunachalam [40].

The applicator achieved a measured effective field size of 21 cm^2 at a depth of 1 cm. Simulation results demonstrated specific absorption rate target coverage of 90% for heterogeneous human body models at various sites. The optimized design enhanced the tangential electric field component to 91% for better power deposition in targeted malignancies. Experimental results confirmed an effective penetration depth of 3 cm, which is suitable for localized skin cancers. A flared conformal water bolus was integrated to eliminate air gaps and ensure uniform heating on irregularly shaped body surfaces. The system achieved a maximum temperature rise of 6°C at 1 cm depth within a 6-minute duration. This heating rate effectively raises the tumor temperature to the therapeutic range of 38–44°C quickly.

A joint optimization method for antenna matching and specific absorption rate focusing in hyperthermia [41]. The phased-array applicator illustrated in Fig. 28 utilizes eight patch antennas arranged in an octagonal circular array immersed within a water bolus coupling medium. Each patch antenna features optimized dimensions of 33.85 mm in length and 7.13 mm wide. Researchers fabricated the system components on I-Tera MT40 substrate layers with a precisely adjusted antenna-to-ground height of 10.5 mm. The system operates at 434 MHz within a standard medical ISM band. This frequency balances electromagnetic energy absorption with adequate penetration depth for treating various deep-seated malignancies. The methodology employs particle swarm optimization to minimize a tailored cost function incorporating active reflection coefficients and target SAR. Simulations were performed using COMSOL Multiphysics, while experimental validation utilized semi-solid agar-based phantoms mimicking realistic human muscle tissues. The designed applicator achieves a penetration depth of 37.32 mm inside the simulated muscle-mimicking phantom material. The effective field size measures 21.49 cm^2 at a depth of 1 cm within the tissue. Optimized feeding coefficients ensure that active reflection coefficients remain below the -10 dB threshold for efficient power transfer. This approach maintains precise energy deposition in the tumor region while effectively minimizing the risk of hotspots in healthy tissues. Furthermore, experimental heating sessions lasted for 130 minutes to reach the desired therapeutic temperature range for effective cancer treatment. The system successfully increased the tumor region temperature to 44°C, as verified by fiber optic sensors.

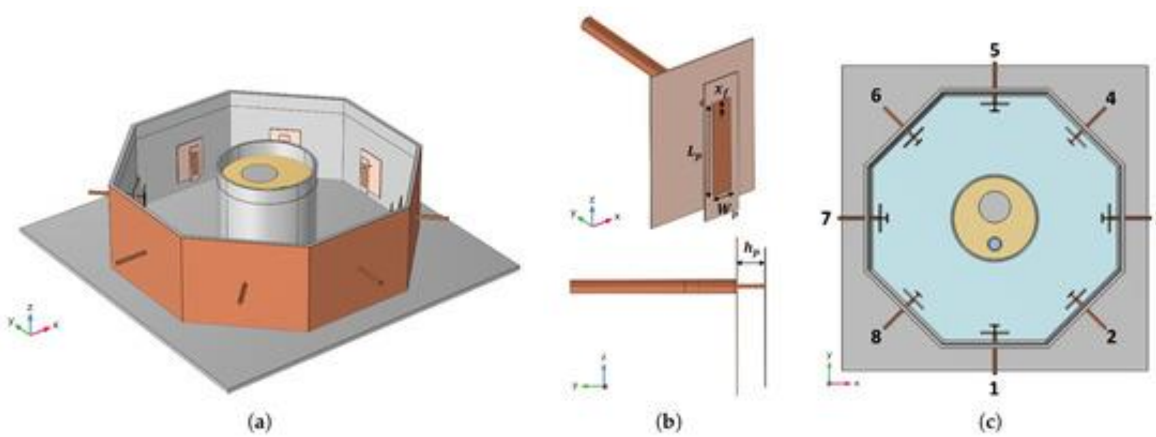

Figure 28.
Hyperthermia Applicator: (a) In-silico Model, (b) Employed Antenna, (c) Top View.
Source: Firuzalizadeh, et al. [41].

Another work was reported in 2025; the authors present a compact dual-band double-spiral antenna [42] as shown in Fig. 29. This multilayer structure features a top spiral radiator, a middle-slotted ground, and a bottom microstrip feed-line component on an FR-4 substrate. Optimization of the three-turn spiral geometry involved 3 mm arm widths and 1.5 mm gaps between adjacent turns. Operating frequencies of 1.8 and 2.45 GHz were selected to target tumors at various tissue depths. The lower frequency provides deeper penetration, while the higher frequency allows for precise localized heating of superficial skin cancer lesions.

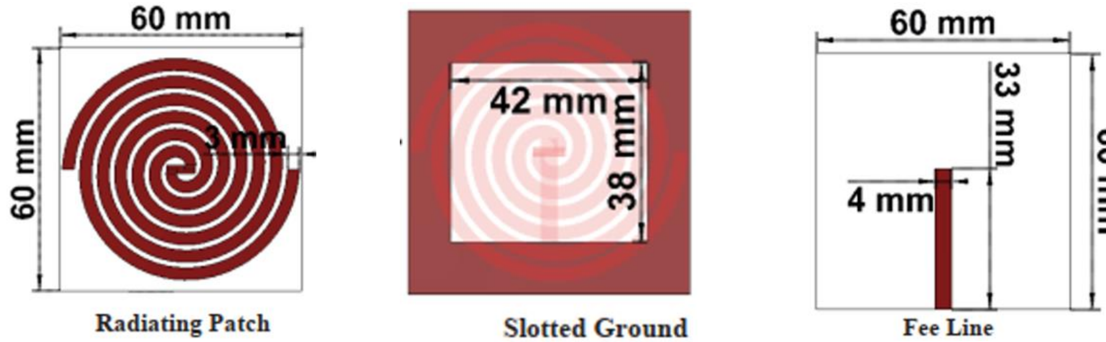

Figure 29.
Multi-Layer Dual-Band Double Spiral Antenna Applicator.
Source: Sharma et al. [42].

SAR analysis achieved a penetration depth of 50 mm at the lower band and 30 mm at the higher band. The effective field size was observed to be 41 x 41 mm² at 1.8 GHz for deeper thermal targeting. At 2.45 GHz, the effective field size increased to 49 × 49 mm² at 10 mm depth. Simulated thermal profiles confirmed that the applicator effectively raised tissue temperatures into the therapeutic range of 40 to 45°C. Experimental testing with a heterogeneous phantom showed a temperature rise from 24 to 28.2°C in 10 minutes. Using 5 W of power increased the phantom temperature to 33.5°C in 340 seconds. These results validate the antenna's capability to deliver safe and controlled thermal energy for localized hyperthermia therapy.

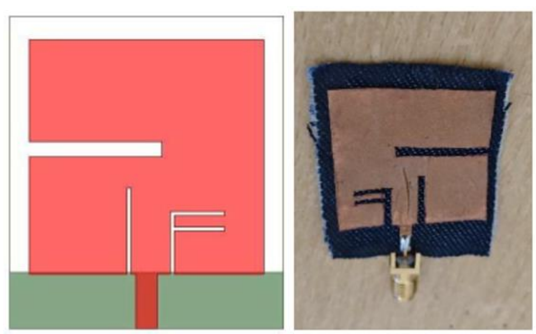

Figure 30.
Antenna Applicator: (a) Final Design, (b) Fabricated Prototype.
Source: Suvartha et al. [43].

Suvartha et al. [43] present a wearable dual-band microstrip patch antenna as shown in Fig. 30. This design features a jeans fabric substrate with a relative permittivity of 1.7 and a thickness of 1.3 mm. The antenna dimensions are 45 mm in length and 30 mm in width for a compact geometry. Researchers utilized an F-shaped slot and a small slot to achieve dual-band resonance and improved impedance matching. The fabrication process involves applying conductive copper tape onto the jeans material and incorporating an SMA connector. The resonant frequencies of the applicator are 2.45 GHz and 7.9 GHz for the heat treatment of cancerous cells in the skin. The lower frequency was selected because electromagnetic waves at this frequency can penetrate deep tissues, such as muscle layers. Conversely, the 7.9 GHz provides localized warming for treating superficial tumors near the skin surface. The integration of dual-band functionality allows for versatile therapy suitable for different types of cancerous tissue regions. The applicator achieves a therapeutic penetration depth of 2–3 cm within various biological human tissues. SAR values are carefully regulated to 1 W/kg to ensure patient safety during exposure. The proposed antenna applicator aims to selectively destroy cancer cells while minimizing damage to the surrounding healthy biological tissues.

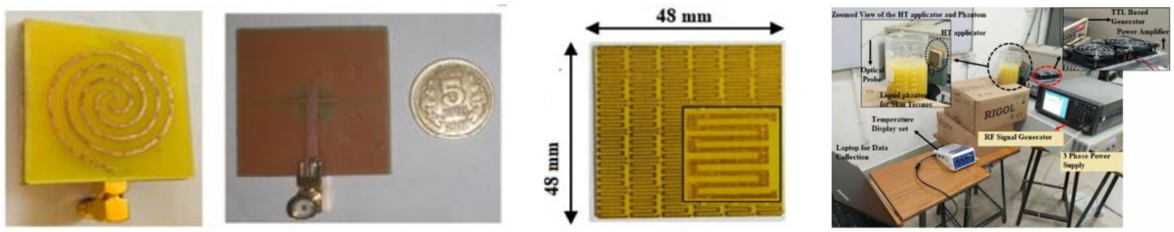

(a) (b) (c)

Figure 31.
Archimedean Applicator: (a) Spiral Antenna, (b) Metamaterial Reflector, (c) Thermal Setup.
Source: Kaur and Kaur [44].

The paper by Kaur and Kaur [44] presents an Archimedean spiral antenna integrated with a 48 x 48 mm^2 epsilon-negative metamaterial reflector, as shown in Fig. 31. The 40 x 40 mm^2 spiral antenna utilizes an aperture-coupled feed that operates effectively within the 2.45 GHz ISM band. The applicator is fabricated on an FR-4 substrate with a thickness of 1.57 mm. An Archimedean spiral radiator comprising two circular spirals, with a strip width of 0.7 mm and a radius of 6.5 mm, is etched on the top surface of the second substrate, while the bottom surface remains free of copper metallization. The first substrate incorporates a microstrip feed line on its bottom surface and an aperture-based defective ground structure on its top surface, enabling excitation of the spiral radiator through an aperture-coupled feeding technique. An epsilon-negative metamaterial reflector is positioned behind the spiral antenna to enhance applicator performance by improving the front-to-back ratio and suppressing backward radiation. The proposed design offers a compact profile, eliminates the need for complex external matching networks, and enhances electromagnetic energy focusing, thereby minimizing undesired heating of healthy tissues during hyperthermia treatment. The applicator achieves a peak SAR of 8 W/kg, a penetration depth (PD) of 32 mm, and an effective field surface (EFS) of 32 × 32 mm^2, demonstrating its suitability for treating deep-seated malignancies. Thermal simulations were performed using input powers of 1 W, 2.5 W, and 3.5 W, demonstrating a tumor temperature rise within the therapeutic range of 41–45°C and uniform heating over an area of up to 36 x 36 mm^2. The target temperature of 43–44°C was achieved within 22 minutes during the simulation, while experimental validation using a tissue-mimicking, semi-liquid phantom confirmed that 45°C could be attained after 40 min of continuous microwave exposure.

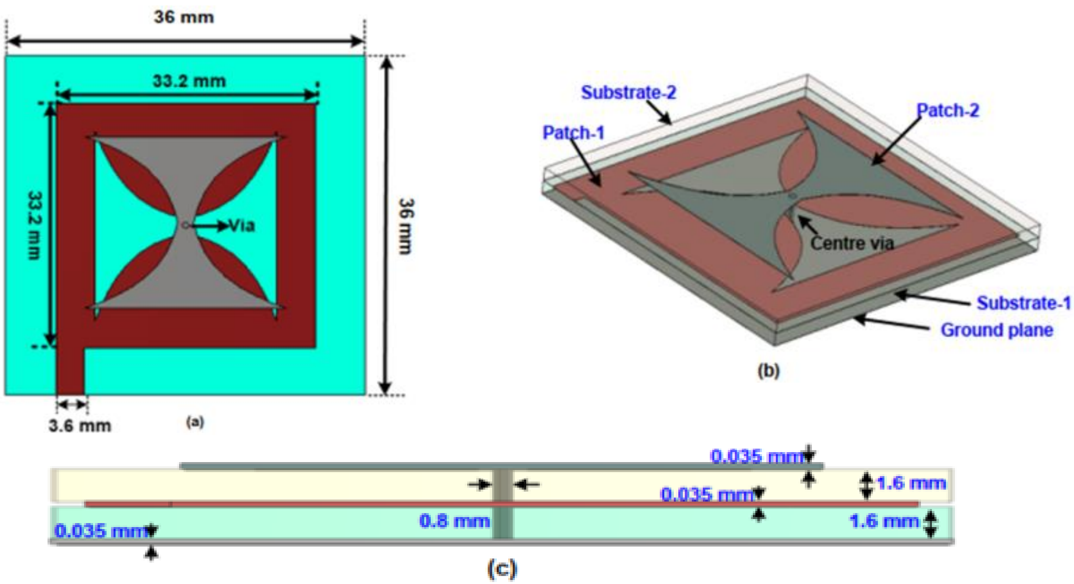

Figure 32.
Antenna Applicator Geometry: (a) Front View, (b) Prospective View, (c) Side View.
Source: Kumari et al. [45].

A novel investigation conducted in 2026 introduces a tapered slot-loaded patch antenna [45], as shown in Fig. 32. This compact, vertically stacked applicator features a symmetrical four-leaf tapered slot layout designed on two distinct FR4 substrate layers. The design maintains an overall footprint of 36 x 36 mm² with a low-profile total height of 3.27 mm. The authors utilized CST Microwave Studio to evaluate the performance within a three-layer heterogeneous phantom representing skin, fat, and muscle. Thermal interactions were accurately assessed by solving Pennes' bioheat transfer equation over a simulation period of 60 minutes. A frequency of 915 MHz was chosen to exploit the dielectric contrast between healthy tissue and malignant skin tumors. The system delivers energy focused within an effective area of exactly 11.8 x 11.8 mm² during target treatment. High-power localization achieves a penetration depth of 22.11 mm when treating a tumor using a five-millimeter water bolus. Continuous input power of 3 W raises the tumor temperature into the therapeutic range of 44°C safely. Utilizing a water bolus protects the skin surface while effectively concentrating electromagnetic energy deeper into the target cancerous region.

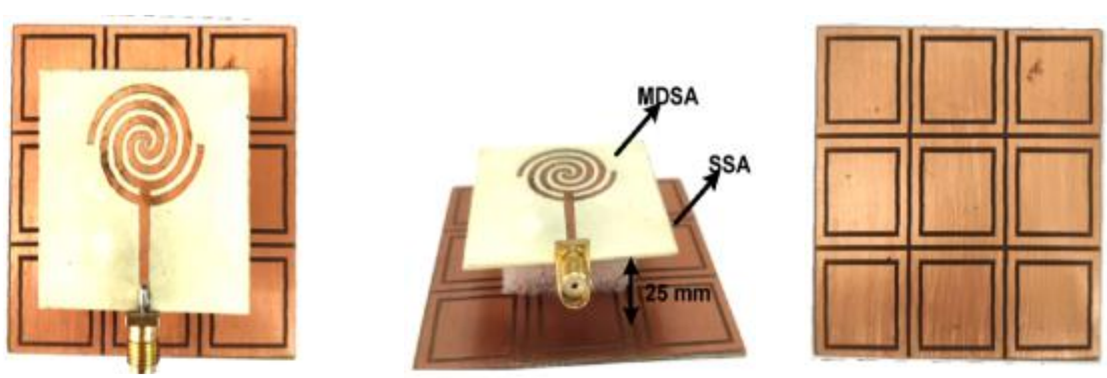

(a) (b) (c)

Figure 33.
Fabricated Prototype of the applicator: (a) Top View, (b) Side View, (c) AMC Reflector.
Source: Sharma et al. [46].

Edelweiss Applied Science and Technology
ISSN: 2576-8484
Vol. 10, No. 9: 21-53, 2026
DOI: 10.55214/2576-8484.v10i9.13548

Another paper Sharma et al. [46] presents a 40 × 40 mm^2 monopole double-spiral antenna operating at 2.45 GHz, integrated with a 60 × 60 mm^2 square-slotted artificial magnetic conductor (AMC)-based reflector for localized superficial hyperthermia, as shown in Fig. 33. The proposed design offers high heating efficiency with low input power, enhanced electric field concentration within the targeted tumor region, and effective suppression of backward radiation to improve localized heating performance. The applicator achieves a maximum SAR of 49.7 W/kg, a penetration depth of 32 mm, and a focused effective field size of 44 × 44 mm^2 for a homogeneous phantom, demonstrating its suitability for localized treatment. Thermal simulations show that an input power of 1 W raises the tumor center temperature to 42°C at a depth of 25 mm, which lies within the therapeutic hyperthermia range. Furthermore, experimental investigations demonstrate that a 1 W input increases the phantom temperature by 6.5°C within 1 minute, while a 2 W input raises the temperature of ex vivo chicken liver tissue to 40°C, confirming the practical feasibility of the proposed applicator.

Table 2.
Comparison of Reported Applicators for Hyperthermia Treatment of Skin & Superficial Cancer.

Ref.	Year	Applicator Type	Freq.	Contributions	Limitations
Tennant, et al. [18]	1990	Robot-controlled Helical Antenna	2.45 GHz	Uniform heating over arbitrary shaped superficial tumor using robotic scanning	No real-time temperature feedback, blood perfusion effects not considered
Montecchia [19]	1992	Disk, Annular-slot & Spiral Microstrip	0.2 – 1 GHz	Compact conformal applicators, Improved heating	Limited coverage
Lee, et al. [20]	1992	5x5 Spiral Microstrip Array	915 MHz	Large-area conformal treatment, Adaptive power control, 3cm PD	Lack of high-resolution thermometry
Cepeda, et al. [21]	2004	Double-slot Coaxial Antenna	2.45 GHz	Interstitial hyperthermia, highly localized heating for deep tumors	Invasive procedure
Safarik and Rychlik [22]	2009	Spiral & Slot Planar Applicators	434 MHz	Flexible planar applicators with improved SAR distribution	Limited heating area
Koo, et al. [23]	2012	Flexible Conformal Microstrip	434 MHz	Flexible multilayer structure with improved conformity	Large physical size
Petrishia and Sasikala [24]	2014	Lens-based Impulse Radiating Antenna	2 – 30 GHz	Ultra-short pulse therapy, highly focused electric field	Non-thermal heating mechanism
Chakaravarthi and Arunachalam [25]	2015	Miniaturized Cavity-backed Folded Patch	434 MHz	Compact cavity-backed antenna, Low penetration depth 8.25mm	Moderate heating depth
Singh and Singh [26]	2015	Microstrip Slot Antenna	2.45 GHz	High penetration and compact geometry	No experimental validation & thermal analysis
Singh and Singh [27]	2015	Water-loaded Diagonal Horn	2.45 GHz	Deep penetration with symmetric SAR	Bulky horn structure
Kim, et al. [28]	2015	8x8 Phased Array	915 MHz	Beam focusing for deep tumors, increased penetration depth	Complex feeding network
Younesiraad, et al. [29]	2017	Dual-band Square Ring Patch	434/915 MHz	Dual-frequency operation with deep penetration	No validation & thermal analysis, Large Antenna
Petrishia [30]	2018	Miniaturized Lens-based PSIRA	2 – 30 GHz	Extremely focused pulsed electric field	Non-thermal heating approach
Tyagi, et al. [31]	2022	Rectangular Spiral Patch	680 MHz	Miniaturized low-frequency applicator	No validation & thermal analysis
Kaur and Kaur [32]	2023	AMC-backed Spiral Applicator	2.45 GHz	Improved penetration depth using AMC reflector	Long heating duration, Structural complexity
Khan, et al. [33]	2023	Dual-band Star Patch	2.45/5.35 GHz	Dual-band operation with high SAR	No experimental validation & thermal Analysis
Gu, et al. [34]	2023	SRR array Applicator	8 – 15 GHz	High-resolution localized heating	High Frequency, very shallow penetration
Alex and	2023	Circular Ring	434 MHz	MRI-based patient model	No validation & thermal

Chakaravarthi [35]		Applicator		validation	analysis, Low PD
Kaur, et al. [36]	2024	Hybrid Fractal Antenna with AMC Reflector & EM Lens	2.45 GHz	Improved beam focusing and bandwidth, Balanced EFS	Multi-layer Fabrication
Duque, et al. [37]	2024	Modified Folded Dipole	2.45 GHz	Water-bolus-free compact applicator	Suitable for localized superficial tumors
Kaur, et al. [38]	2025	Flexible Double Spiral Antenna	915 MHz	Flexible PET-based applicator with moderate penetration depth	No thermal analysis, Narrow bandwidth
Khan, et al. [39]	2025	C & T Slotted Patch Antenna	915 MHz	High SAR at shallow depth	No validation & thermal analysis, Low PD
Choudhary and Arunachalam [40]	2025	Water-loaded Folded Patch	434 MHz	Improved coupling using conformal water bolus, Compact cavity-backed applicator	Requires water bolus
Firuzalizadeh, et al. [41]	2025	Phased Array Applicator	434 MHz	Hotspot reduction, Joint antenna matching and SAR optimization	Long treatment duration
Sharma, et al. [42]	2025	Dual-band Double Spiral	1.8/2.45 GHz	Multi-depth heating capability	Experimental temp. below therapeutic range
Suvartha, et al. [43]	2025	Dual-band Textile Antenna	2.45/7.9 GHz	Wearable textile-based applicator	No thermal Analysis, Low SAR
Kaur and Kaur [44]	2025	Archimedean Spiral Applicator with ENG MM Reflector	2.45 GHz	Compact metamaterial-assisted applicator with improved energy focusing, deep penetration, uniform heating	No clinical & ex-vivo validation
Kumari, et al. [45]	2026	Tapered Slot-loaded Patch	915 MHz	Compact stacked design with focused heating, Small EFS	No experimental validation
Sharma, et al. [46]	2026	Monopole Double-Spiral Antenna with AMC Reflector	2.45 GHz	Compact applicator with high efficiency, suppressed backward radiation, and therapeutic heating using only 1W input power	No clinical validation

5. Conclusion

Microwave hyperthermia has emerged as a promising invasive and non-invasive adjunct therapy for the effective treatment of cancers. This review comprehensively summarizes the evolution of microwave hyperthermia applicators reported from 1990 to 2026 for skin and superficial cancer treatment. The reviewed studies demonstrate conventional waveguide, microstrip applicators, compact & conformal applicators, phased-array, wearable, and metamaterial-based applicators with improved therapeutic performance. Table 2 highlights the selected operating frequency, contributions, and limitations of reported applicators for skin and superficial tumors. The comparison also reveals that many reported designs still lack experimental validation, thermal characterization, real-time temperature monitoring, and clinically relevant performance assessment. Although phased-array and metamaterial-based applicators improve heating uniformity and penetration depth, their structural complexity, large dimensions, and complex feeding networks remain practical limitations. Therefore, future research should focus on compact, patient-specific, and experimentally validated hyperthermia applicators that would be capable of achieving safe, precise, and clinically reliable cancer treatment.

Transparency:

The authors confirm that the manuscript is an honest, accurate, and transparent account of the study; that no vital features of the study have been omitted; and that any discrepancies from the study as planned have been explained. This study followed all ethical practices during writing.

Acknowledgement:
The authors gratefully acknowledge the financial assistance provided by the Indian Council for Medical Research (ICMR), India, through the research grant (File No. 17X(3)/Adhoc/3/2022-ITR) with a sanctioned amount of INR 68.68 lakhs, which supported this work.

References
[1] D. Nandakumar, R. Dixit, and M. Pandey, "Cancer prevention through lifestyle modification," *The Indian Journal of Medical Research*, vol. 161, no. 2, pp. 109-111, 2025. https://doi.org/10.25259/IJMR_405_2025
[2] L. A. Torre, F. Bray, R. L. Siegel, J. Ferlay, J. Lortet-Tieulent, and A. Jemal, "Global cancer statistics, 2012," *CA: A Cancer Journal for Clinicians*, vol. 65, no. 2, pp. 87-108, 2015. https://doi.org/10.3322/caac.21262
[3] Z. Apalla, D. Nashan, R. B. Weller, and X. Castellsagué, "Skin cancer: Epidemiology, disease burden, pathophysiology, diagnosis, and therapeutic approaches," *Dermatology and Therapy*, vol. 7, no. Suppl 1, pp. 5-19, 2017. https://doi.org/10.1007/s13555-016-0165-y
[4] National Cancer Institute, "Skin cancer treatment (PDQ)–patient version, Bethesda, MD, USA," 2025. https://www.cancer.gov/types/skin/patient/skin-treatment-pdq
[5] D. Schadendorf *et al.*, "Melanoma," *The Lancet*, vol. 392, no. 10151, pp. 971-984, 2018. https://doi.org/10.1016/S0140-6736(18)31559-9
[6] A. Mirbeik, R. Ashinoff, T. Jong, A. Aued, and N. Tavassolian, "Real-time high-resolution millimeter-wave imaging for in-vivo skin cancer diagnosis," *Scientific Reports*, vol. 12, no. 1, p. 4971, 2022. https://doi.org/10.1038/s41598-022-09047-6
[7] T. P. Ryan and C. L. Brace, "Interstitial microwave treatment for cancer: Historical basis and current techniques in antenna design and performance," *International Journal of Hyperthermia*, vol. 33, no. 1, pp. 3-14, 2017. https://doi.org/10.1080/02656736.2016.1214884
[8] National Cancer Institute, "Hyperthermia to treat cancer, Bethesda, MD, USA," 2025. https://www.cancer.gov/about-cancer/treatment/types/hyperthermia
[9] B. Hildebrandt *et al.*, "The cellular and molecular basis of hyperthermia," *Critical Reviews in Oncology/Hematology*, vol. 43, no. 1, pp. 33-56, 2002. https://doi.org/10.1016/S1040-8428(01)00179-2
[10] American Cancer Society, "Hyperthermia to treat cancer, Atlanta, GA, USA," 2025. https://www.cancer.org/cancer/managing-cancer/treatment-types/hyperthermia.html
[11] M. H. Falk and R. D. Issels, "Hyperthermia in oncology," *International Journal of Hyperthermia*, vol. 17, no. 1, pp. 1-18, 2001. https://doi.org/10.1080/02656730118511
[12] P. Wust *et al.*, "Hyperthermia in combined treatment of cancer," *The Lancet Oncology*, vol. 3, no. 8, pp. 487-497, 2002. https://doi.org/10.1016/S1470-2045(02)00818-5
[13] S. Singh, S. P. Singh, and S. Singh, "External microwave applicators for hyperthermia therapy: A review," *Discover Applied Sciences*, vol. 7, no. 3, p. 198, 2025. https://doi.org/10.1007/s42452-025-06621-1
[14] S. Montoya-Villada, E. Reyes-Vera, and J. Orozco, "Microwave technologies for biomedical diagnosis and therapy: Advances, challenges, and perspectives," *Microchimica Acta*, vol. 193, no. 4, p. 218, 2026. https://doi.org/10.1007/s00604-025-07826-2
[15] J. Van der Zee, "Heating the patient: A promising approach?," *Annals of Oncology*, vol. 13, no. 8, pp. 1173-1184, 2002. https://doi.org/10.1093/annonc/mdf280
[16] N. Malhotra, A. Marwaha, and A. Kumar, "Accurate investigation of coaxial-slot antenna for invasive microwave hyperthermia therapy," *International Journal of Sciences: Basic and Applied Research*, vol. 16, no. 1, pp. 388–396, 2014.
[17] R. L. Magin and A. F. Peterson, "Invited review: Noninvasive microwave phased arrays for local hyperthermia: A review," *International Journal of Hyperthermia*, vol. 5, no. 4, pp. 429-450, 1989. https://doi.org/10.3109/02656738909140470
[18] A. Tennant, J. Conway, and A. Anderson, "A robot-controlled microwave antenna system for uniform hyperthermia treatment of superficial tumours with arbitrary shape," *International Journal of Hyperthermia*, vol. 6, no. 1, pp. 193-202, 1990. https://doi.org/10.3109/02656739009140815
[19] F. Montecchia, "Microstrip-antenna design for hyperthermia treatment of superficial tumors," *IEEE Transactions on Biomedical Engineering*, vol. 39, no. 6, pp. 580-588, 1992. https://doi.org/10.1109/10.141196
[20] E. R. Lee *et al.*, "Body conformable 915 MHz microstrip array applicators for large surface area hyperthermia," *IEEE Transactions on Biomedical Engineering*, vol. 39, no. 5, pp. 470-483, 1992. https://doi.org/10.1109/10.135541

[21] M. Cepeda, A. Vera, and L. Leija, "Microcoaxial Double slot antenna for interstitial hyperthermia: Design, modeling and validation," in *2008 International Conference on Advances in Electronics and Micro-electronics (pp. 138-143). IEEE*, 2008.

[22] J. Safarik and O. Rychlik, "Planar applicators for local hyperthermia," in *2009 19th International Conference Radioelektronika (pp. 349-352). IEEE*, 2009.

[23] Y. S. Koo, A. E. Fathy, R. Kazemi, and J. Phillips, "Construction of a conformal applicator for hyperthermia treatment of superficial skin cancer," in *Proceedings of the 2012 IEEE International Symposium on Antennas and Propagation (pp. 1-2). IEEE*, 2012.

[24] A. Petrishia and M. Sasikala, "Design of tapered arm impulse radiating antenna with log periodic lens system for skin cancer treatment," *Journal of Medical Engineering & Technology*, vol. 38, no. 3, pp. 135-145, 2014. https://doi.org/10.3109/03091902.2014.884180

[25] G. Chakaravarthi and K. Arunachalam, "Design and characterisation of miniaturised cavity-backed patch antenna for microwave hyperthermia," *International Journal of Hyperthermia*, vol. 31, no. 7, pp. 737-748, 2015. https://doi.org/10.3109/02656736.2015.1068957

[26] S. Singh and S. Singh, "Microstrip slot antenna for hyperthermia applications," in *2015 IEEE Applied Electromagnetics Conference (AEMC) (pp. 1-2). IEEE*, 2015.

[27] S. Singh and S. P. Singh, "Water-loaded metal-dielectric wall diagonal horn antenna for hyperthermia application," in *2015 IEEE 15th Mediterranean Microwave Symposium (MMS) (pp. 1-4). IEEE*, 2015.

[28] K. J. Kim, W. C. Choi, Y. J. Yoon, and S.-h. Bae, "Planar array for non-invasive ultra-superficial hyperthermia applicator," in *2015 International Workshop on Antenna Technology (iWAT) (pp. 104-106). IEEE*, 2015.

[29] H. Younesiraad, M. Bemani, and S. Nikmehr, "A dual-band slotted square ring patch antenna for local hyperthermia applications," *Progress in Electromagnetics Research Letters*, vol. 71, pp. 97-102, 2017. https://doi.org/10.2528/PIERL17090503

[30] A. Petrishia, "Design of compact lens system for miniaturized prolate spheroidal impulse radiating antenna for skin cancer treatment," *Progress in Electromagnetics Research M*, vol. 70, pp. 41-50, 2018. https://doi.org/10.2528/PIERM18051101

[31] P. Tyagi, K. Bajpai, R. Dwivedi, N. Sharma, and P. Mudgal, "Patch antenna for microwave hyperthermia applications," presented at the 2nd International Conference on Advancement in Electronics & Communication Engineering, 2022.

[32] K. Kaur and A. Kaur, "Metamaterial based AMC backed archimedean spiral antenna for in-vitro microwave hyperthermia of skin cancer," *Electromagnetic Biology and Medicine*, vol. 42, no. 4, pp. 163-181, 2023. https://doi.org/10.1080/15368378.2023.2297954

[33] A. Khan, A. Mishra, S. Dubey, and A. Singh, "Design of a Dual ISM Band Antenna at 2.5 GHz and 5.35 GHz for hyperthermia application," in *2023 International Conference on Microwave, Optical, and Communication Engineering (ICMOCE) (pp. 1-4). IEEE*, 2023.

[34] Y. Gu, D. Kendig, M. Shakouri, and D. W. van der Weide, "Dual mode split ring resonator sensing and hyperthermia array for skin," *IEEE Journal of Electromagnetics, RF and Microwaves in Medicine and Biology*, vol. 8, no. 3, pp. 206-212, 2024. https://doi.org/10.1109/JERM.2024.3373537

[35] M. Alex and G. Chakaravarthi, "Circular ring microwave applicator for superficial hyperthermia treatment," in *2023 IEEE Microwaves, Antennas, and Propagation Conference (MAPCON) (pp. 1-4). IEEE*, 2023.

[36] K. Kaur, A. Kaur, A. Pattanayak, and D. Choudhury, "A metamaterial backed hybrid fractal microstrip patch antenna, integrated with an EM lens for non-invasive hyperthermia of skin cancer," *Optical and Quantum Electronics*, vol. 56, no. 12, p. 1973, 2024. https://doi.org/10.1007/s11082-024-07746-0

[37] J. Duque, I. Díaz, and J. Araque, "Thermal validation of a novel antenna design for superficial microwave hyperthermia," in *2024 IEEE 1st Latin American Conference on Antennas and Propagation (LACAP) (pp. 1-2). IEEE*, 2024.

[38] N. Kaur, A. Bansal, G. Singla, H. Gupta, and R. Khanna, "Non-invasive spiral antenna applicator for hyperthermia application of skin/neck cancer," in *2025 IEEE Microwaves, Antennas, and Propagation Conference (MAPCON) (pp. 1-4). IEEE*, 2025.

[39] A. Khan, A. Mishra, and A. K. Singh, "Advancing hyperthermia applications: Design and analysis of an orthogonal C and T Slot ISM band antenna," in *2025 International Conference on Electrical, Communication, and Computing Technologies (iCONECCT) (pp. 1-4). IEEE*, 2025.

[40] R. Choudhary and K. Arunachalam, "Dielectric loaded antenna with conformal waterbolus and improved SAR for hyperthermia treatment of localized superficial cancer," *Ieee Access*, vol. 13, pp. 66878-66887, 2025. https://doi.org/10.1109/ACCESS.2025.3558614

[41] M. Firuzalizadeh *et al.*, "Joint optimization of antenna system matching and specific absorption rate focusing in microwave hyperthermia cancer treatment," *Cancers*, vol. 17, no. 3, p. 386, 2025. https://doi.org/10.3390/cancers17030386

[42] N. Sharma, R. Khanna, M. K. Rai, and K. Kumari, "Development of a dual-band double spiral antenna for medical hyperthermia therapy," in *2025 5th Asian Conference on Innovation in Technology (ASIANCON) (pp. 1-7). IEEE*, 2025.

[43] P. Suvartha, K. H. V. Raju, B. Sudhakar, G. Usha, and P. V. Reddy, "A design of dual-band and flexible microstrip patch antenna for cancer hyperthermia therapy in biomedical applications," in *International Conference on Computer Science and Communication Engineering (ICCSCE 2025) (pp. 2833-2840). Atlantis Press*, 2025.

[44] K. Kaur and A. Kaur, "An Archimedean spiral antenna integrated with an epsilon-negative metamaterial reflector as microwave hyperthermia applicator for non-invasive treatment of early-stage skin cancer," *International Journal of Biomedical Engineering and Technology*, vol. 49, no. 3, pp. 233-262, 2025. https://doi.org/10.1504/IJBET.2025.150064

[45] K. Kumari, N. Sharma, R. Khanna, and M. K. Rai, "Tapered slot loaded patch antenna for superficial skin cancer treatment," in *2026 6th International Conference on Image Processing and Capsule Networks (ICIPCN) (pp. 1144-1149). IEEE*, 2026.

[46] N. Sharma, R. Khanna, and M. K. Rai, "SAR-enhanced hyperthermia applicator for localized superficial tumors with temperature profiling in ex vivo biological tissue," *International Journal of Thermal Sciences*, vol. 228, p. 111029, 2026. https://doi.org/10.1016/j.ijthermalsci.2026.111029

Edelweiss Applied Science and Technology
ISSN: 2576-8484
Vol. 10, No. 9: 21-53, 2026
DOI: 10.55214/2576-8484.v10i9.13548